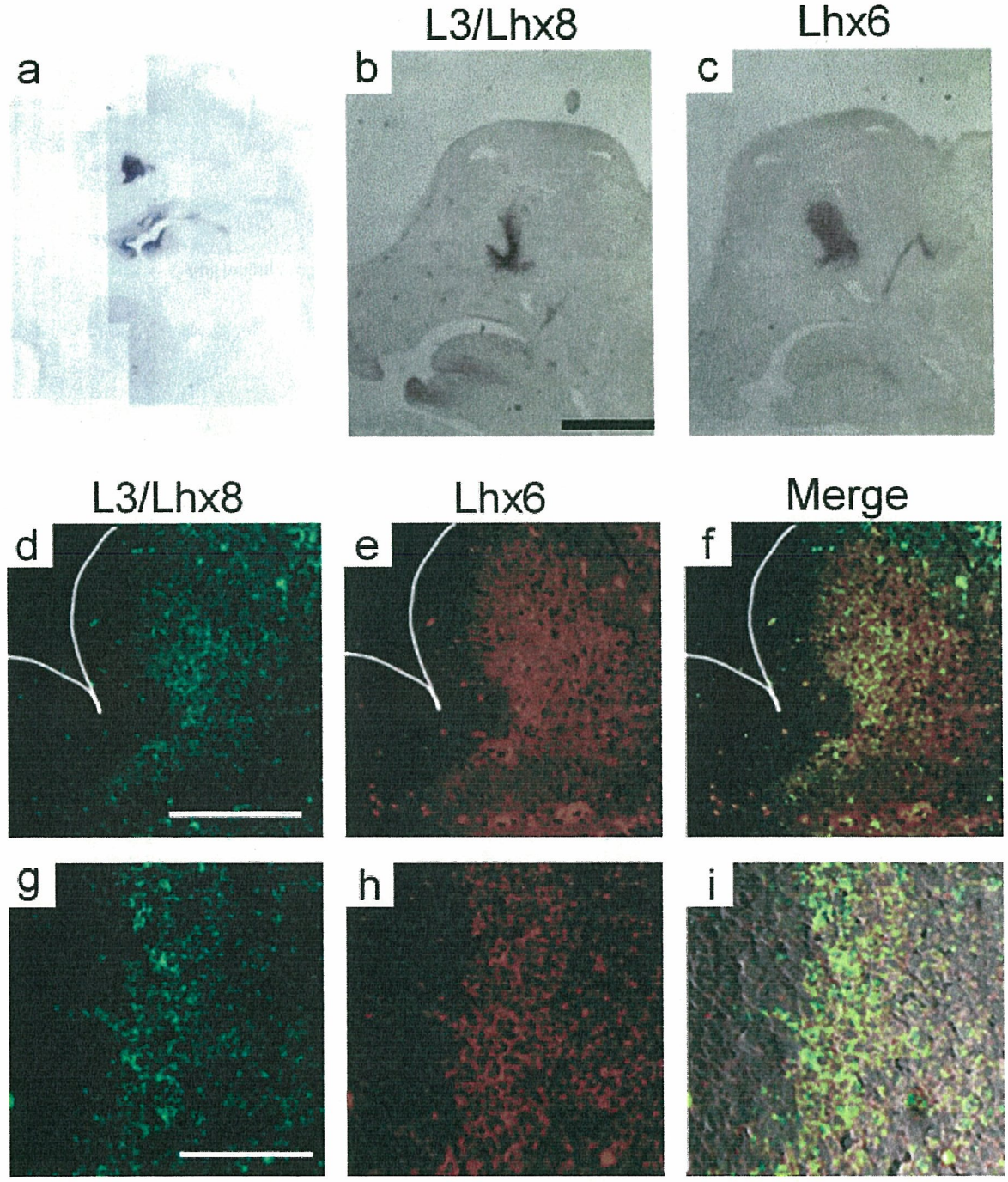

FIG. 1. *L3/Lhx8* and *Lhx6* mRNAs are expressed in developing basal forebrain. The *L3/Lhx8* mRNA expression domain is included in that of *Lhx6*. (a) *L3/Lhx8* mRNA is expressed in the medial ganglionic eminence (MGE) and mesenchymal cells in the upper and lower jaws (JAWS). A sagittal section of the wild type (WT) E12.5 embryo was hybridized with an *L3/Lhx8* full-length probe. (b and c) The *L3/Lhx8* mRNA expression domain is included in that of *Lhx6* in the MGE and *L3/Lhx8* mRNA is expressed in a relatively more anterior part of the MGE than *Lhx6*. The scale bar in (a) represents 1 mm, also for (c). Serial sagittal sections of an E12.5 embryo were hybridized with an *L3/Lhx8* full-length probe (b) or *Lhx6* probe (c). (d–i) *L3/Lhx8* and *Lhx6* mRNAs are co-localized in the same cells in the MGE. Double-labelling fluorescence *in situ* hybridization was performed on the same coronal section of the E12.5 embryo; green, *L3/Lhx8* probe (c and g); red, *Lhx6* probe (e and h); and merged (f and i). Double-positive cells are yellow. Panels (g)–(i) are higher-magnification photographs of (d)–(f), respectively. The scale bar in (d) represents 50 μm, and for (e) and (f). The scale bar in (g) represents 25 μm, and for (h) and (i).

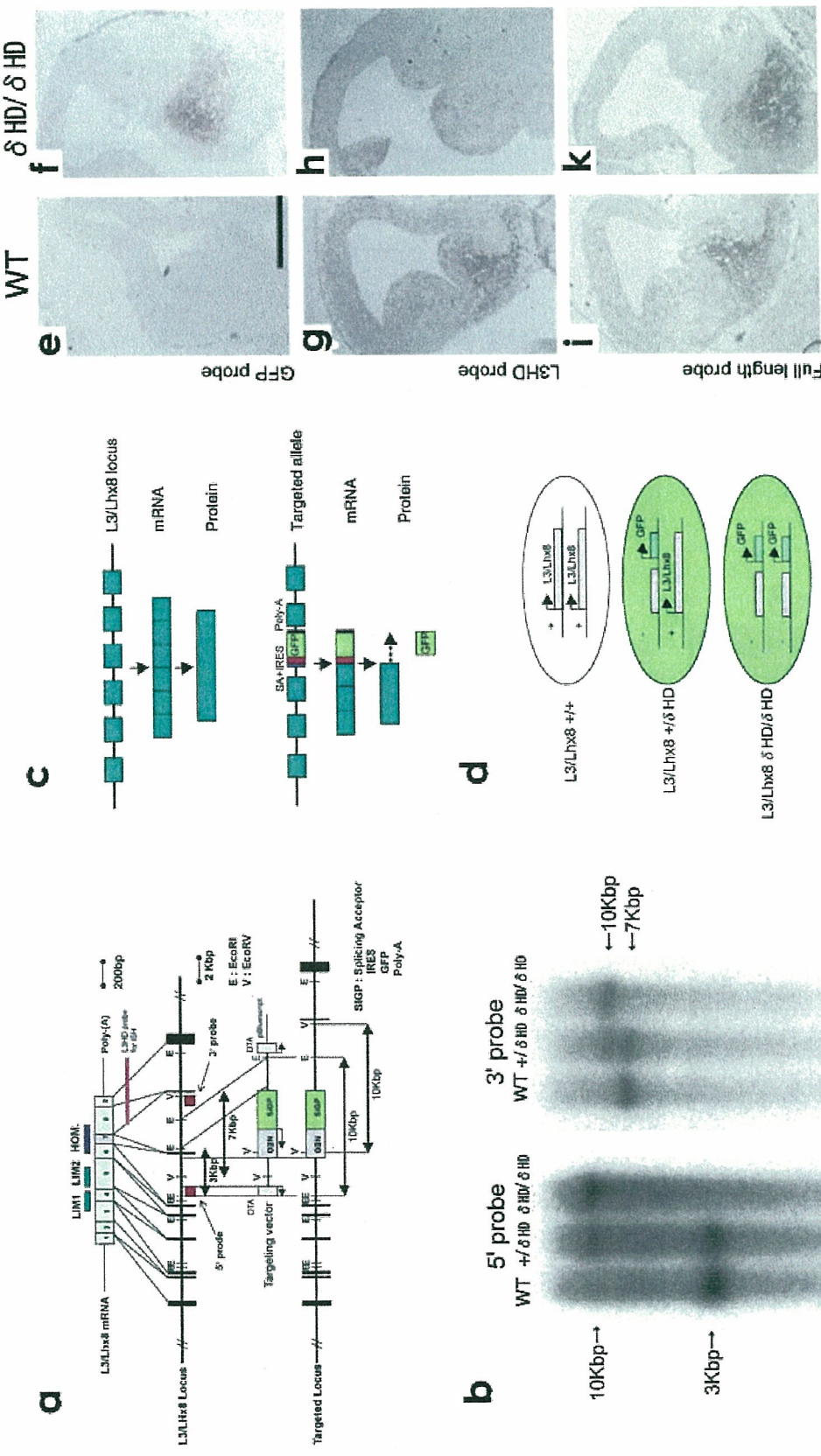

FIG. 2. *L3/Lhx8* targeting strategy and genotyping. (a) A restriction map of the genomic region containing *L3/Lhx8* is shown at the top with the relative positions of each exon. The targeting vector (middle) and the targeted locus (bottom) are also shown. (b) Genotyping of the embryos from the *L3/Lhx8*+/δHD intercross analysed by Southern blotting. *Eco*RI- (left) or *Eco*RV- (right) digested genomic DNAs were hybridized with an external 5′ probe or 3′ probe, respectively. The 5′ probe recognizes the 3-kbp wild type allele and the 10-kbp targeted allele. The 3′ probe recognizes the 7-kbp wild type allele and the 10-kbp targeted allele. RI, *Eco*RI; V, *Eco*RV; *NEO*, neomycin-resistant gene cassette; *SIGP*, *green fluorescent protein* (*GFP*) expression cassette (see Materials and methods and below). Fusion mRNA consisting of tandem LIM domains of *L3/Lhx8* and eGFP mRNAs is expressed from the targeted allele. (c) Scheme of eGFP protein expression from the *SIGP* (*Splicing acceptor* + *IRES* + *eGFP* + *PolyA signal*) cassette. Fusion mRNA with tandem LIM domains and eGFP would be transcribed by the splicing acceptor. From this fusion mRNA, LIM domain-only protein and, simultaneously, eGFP protein would be translated via *IRES*. (d) As a result, heterozygous and homozygous cells express *eGFP* from the targeted allele. eGFP mRNA is expressed in heterozygous (data not shown) and homozygous mice (f), but not in the WT mice (e). The homeodomain-specific (*L3HD*) probe does not label homozygous MGE (h), but does label WT (g) and heterozygous (data not shown) MGE. By contrast, the full-length probe of *L3/Lhx8* labels WT (i), heterozygous (data not shown) and homozygous (k) MGE. The scale bar in (c) represents 500 μm for all panels.

M-MLV RTase from 5 μg total RNA. PCR was performed with the primers described previously (Lopez-Coviella *et al.*, 2000).

Results

Characterization of L3/Lhx8 *δHD mice*

L3/Lhx8 mRNA was expressed in the medial ganglionic eminence (MGE) and the mesenchyme around the oral cavity (Matsumoto *et al.*, 1996; Zhao *et al.*, 1999) (Fig. 1a). *Lhx6* is closely related to *L3/Lhx8* and has a similar gene-expression profile; these two genes could have a redundant role in developing mice (Grigoriou *et al.*, 1998; Zhang *et al.*, 2002) (Fig. 1b and c). Double-labelling FISH indicated that their mRNAs were co-localized in the MGE (Fig. 1d–i). A notable point was that the *L3/Lhx8* mRNA expression domain was included within the *Lhx6* mRNA expression domain (Asbreuk *et al.*, 2002) (Fig. 1b–i). We therefore designed a targeting vector to disrupt the *L3/Lhx8* function and to limit simultaneously possible compensational effects of *Lhx6* (see Materials and methods, Fig. 2a)

Heterozygous (δHD/+) mice appeared normal and these animals mated to produce homozygous mutants. Progenies intercrossed between heterozygous mice were genotyped after weaning. We found that only 14 (3.76%) were δHD/δHD out of 372 offspring after weaning. Judging from the ratio of genotypes of embryos, δHD/δHD mutants were not embryonic lethal and so were born alive (Table 1). Their appearances and spontaneous motions were indistinguishable from WT and δHD/+ mice (data not shown), but most died within several hours, possibly due to a complete cleft of the secondary palate. The incidence rate of cleft palate among the δHD/δHD mutants was about 94% on postnatal day (P) 0; however, mutants without cleft palate (5.6%) could survive to adulthood (P30) (Table 1). The rate was clearly different from that (60%) of the previous −/− mice (Zhao *et al.*, 1999). Other craniofacial features of the δHD/δHD mutants (mandible, maxilla, teeth, tongue, etc.) appeared normal. The craniofacial phenotypes of the δHD/δHD mice will be described in detail elsewhere.

We could not detect an eGFP protein expression from targeted alleles under fluorescent microscopy or by immunohistochemistry with an anti-GFP antibody. Because *eGFP* mRNA expression was confirmed by ISH with an *eGFP* probe (Fig. 2f) and the expression pattern was similar to that of *L3/Lhx8* mRNA in WT mice (Fig. 2g and i), we speculate that the translation efficiency of *eGFP* is very low or it may be suppressed in the mice for some unknown reason. In the δHD/δHD mice, we could detect ISH signals with an *L3/Lhx8* full-length probe (Fig. 2j) but not with an HD probe (Fig. 2h). These results indicate that mRNA for the LIM domain of L3/Lhx8 protein is expressed from the targeted allele.

Molecular marker expression in the basal forebrain of δHD/δHD mice

To check whether patterning within the developing ventral telencephalon of δHD/δHD mice is altered, we compared expression patterns of several molecular markers between WT, δHD/+ and δHD/δHD mice by ISH histochemistry. The following probes were used as markers of the ventral telencephalon: *Dlx2* [ventricular zone (VZ) and subventricular zone (SVZ) of lateral and medial ganglionic eminence (LGE and MGE)] (Eisenstat *et al.*, 1999) (Fig. 3a and b); *Dlx5* (SVZ and mantle layer of LGE and MGE) (Eisenstat *et al.*, 1999) (Fig. 3c and d); *Nkx2.1* (whole MGE) (Marin *et al.*, 2002) (Fig. 3e and f); *Lhx6* (SVZ and mantle layer of MGE) (Grigoriou *et al.*, 1998; Kimura *et al.*, 1999) (Fig. 3g and h); and *Gbx2* (mantle layer of MGE) (Bulfone *et al.*, 1993) (Fig. 3i and j). In addition, *Shh* (mantle layer of MGE) (Kohtz *et al.*, 1998) (Fig. 3k and l) and its signalling components, *Ptc* (VZ most prominent in MGE) (Fig. 3m and n) and *Smo* (VZ) (Fig. 3o and p) mRNA expressions were examined, because Shh signalling is essential for the establishment of the ventral forebrain (Ericson *et al.*, 1995; Kohtz *et al.*, 1998). As illustrated in Fig. 3, none of the marker expression patterns changed in δHD/δHD mice as compared with WT or heterozygous mice.

Cholinergic neurons decreased in the basal forebrain of δHD/δHD mice

Because most BFCNs in adults express *L3/Lhx8* (Asbreuk *et al.*, 2002), we next examined several cholinergic marker expressions in δHD/δHD mice. At P0, we could not detect any cholinergic marker expressions in the basal forebrain; the markers included VAChT (Fig. 4e–h), p75 – a low-affinity NGF receptor (Fig. 4i–l), ChAT (data not shown) and choline transporter-1, CHT-1 (Misawa *et al.*, 2001) (data not shown). It should be noted that in other central nervous system regions, such as the spinal cord motor neurons, the marker expressions were similar between WT and δHD/δHD mice (Fig. 4m and n).

In the homozygous adults that survived (Table 1), we were able to detect ChAT-immunopositive cells in the basal forebrain, but the numbers were greatly diminished compared with WT or heterozygous mice (Fig. 5a–h). When we counted the cholinergic neurons per nuclei of the basal forebrain, the extent of the reduction varied between each nucleus in the homozygous mice as compared with WT mice (see Fig. 9). There are two possible explanations for this reduction: first, BFCNs of the homozygous mice died in a necrotic or apoptotic manner, and second, they changed their transmitter phenotype during development. We currently favour the latter hypothesis. The *GFP* mRNA expression pattern in the homozygous mice (Fig. 2f) was very similar to that of *L3/Lhx8* in the WT or heterozygous mice (Fig. 2i),

TABLE 1. *L3/Lhx8* δHD/δHD mice were not embryonic lethal

Stage	Total	WT (*n*)	WT (%)	+/δHD (*n*)	+/δHD (%)	δHD/δHD (*n*)	δHD/δHD (%)	δHD/δHD with cleft palate	δHD/δHD with normal palate
E12.5	88	31	35.2	39	44.3	18	20.5	–	–
E14.5	383	107	27.9	189	49.3	87	22.7	–	–
E16.5	57	16	28.1	27	47.4	14	24.6	–	–
E18.5	48	15	31.3	21	43.8	12	25.0	–	–
P0	178	50	28.1	75	42.1	53	29.8	50	3
P30	–	–	–	–	–	–	–	0	3

Heterozygous mice were intercrossed and their progenies genotyped at each stage. Homozygous embryos are present in the expected mendelian ratio of roughly 25% during the embryonic stage. Among 53 homozygous mice on P0, only three exhibit a normal palate and survive to adulthood (P30). The incidence of cleft palate among homozygous mice was about 94%. The morning of the appearance of the copulation plug was defined as E0.5.

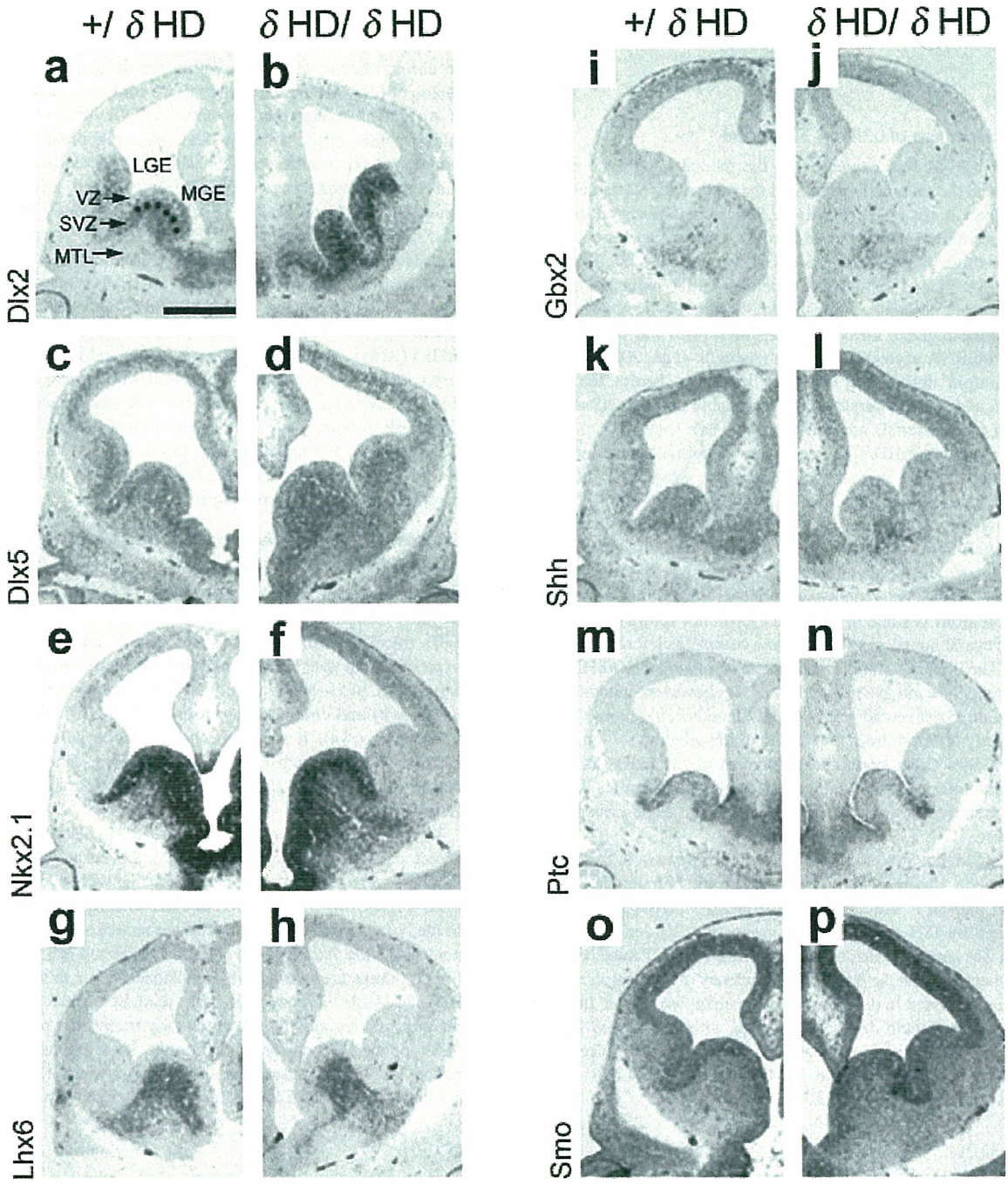

FIG. 3. Molecular marker expression patterns in developing basal forebrain. *In situ* hybridization histochemistry was performed with coronal sections of E12.5 embryos from heterozygous (a, c, e, g, i, k, m and o) and homozygous (b, d, f, h, j, l, n and p) mice. Because the expression patterns are comparable between WT and heterozygous mice, only heterozygous mice are shown in this figure as controls. The markers are indicated at the left of each paired panel: *Dlx2* (a, b), *Dlx5* (c and d), *Nkx2.1* (e and f), *Lhx6* (g and h), *Gbx2* (i and j), *Sonic hedgehog* (k and l), *Patched* (m and n) and *Smoothened* (o and p). Shh, *sonic hedgehog*; Ptc, *patched*; Smo, *smoothened*; VZ, ventricular zone; SVZ, subventricular zone; MTL, mantle layer. The scale bar in (a) represents 500 μm for all panels.

strongly suggesting that neurons expressing GFP in the basal forebrain did not die but transformed to a phenotype other than cholinergic in *L3/Lhx8* δHD/δHD mice. In view of this hypothesis, we next examined distributions of several neurotransmitters, i.e. *enkephalin* (Fig. 6a and b), *neuropeptide Y* (Fig. 6c and d), *somatostatin* (Fig. 6e and f), *substance P* (Fig. 6g and h), galanin (data not shown) and *GAD* (data not shown) of P0 and adult mice (data not shown) in the basal forebrain. No significant changes of their mRNA expressions were observed.

It has been shown that bone morphogenetic proteins (BMPs), especially *BMP-9*, induce and maintain the cholinergic phenotype in the basal forebrain (Lopez-Coviella *et al.*, 2000). We therefore examined *BMP-9* mRNA expression in the E14.5 basal forebrain of all the genotypes with RT-PCR. BMP-9 mRNA was always detected (Fig. 7).

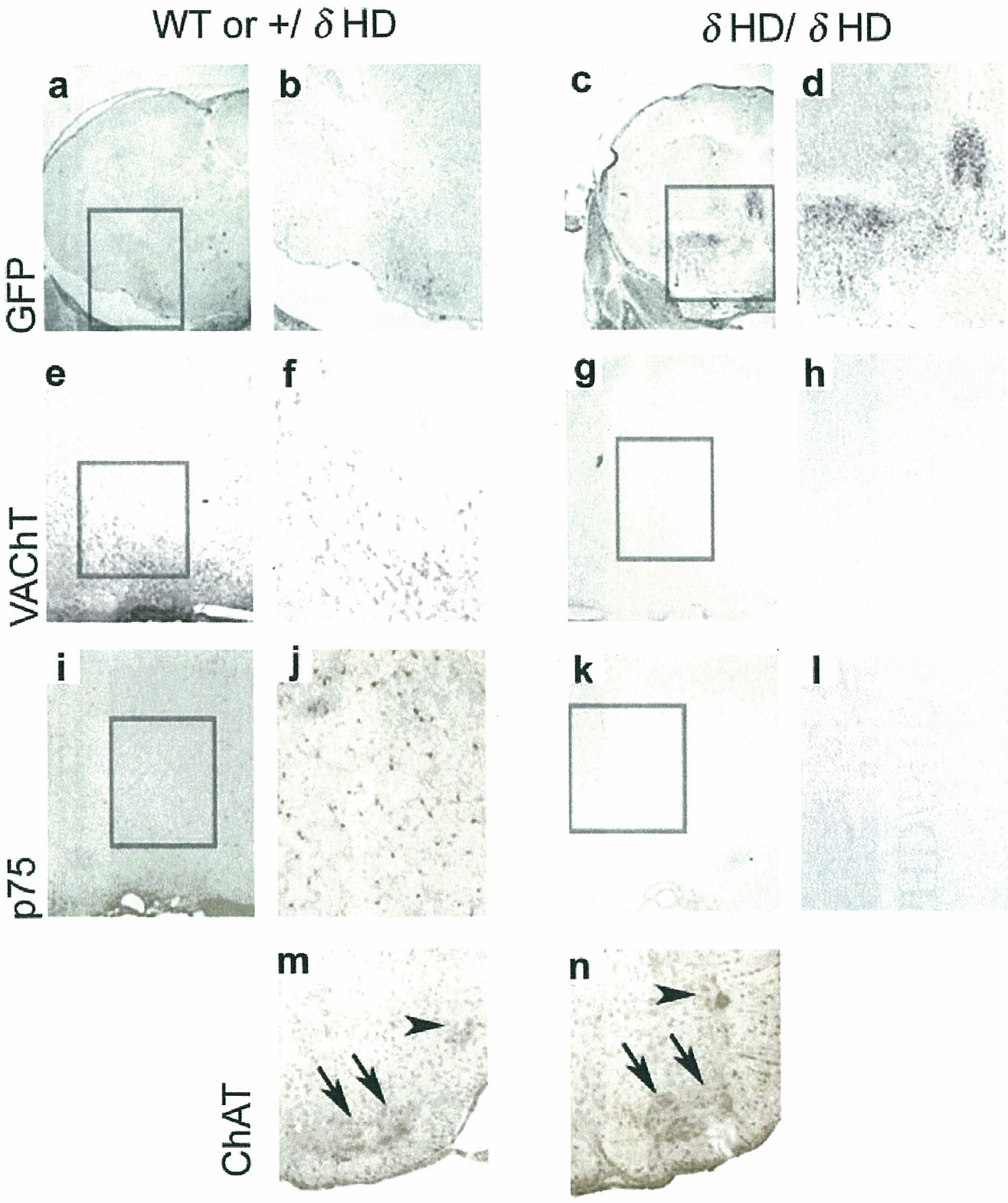

FIG. 4. Cholinergic neuron marker expressions are not detected in the basal forebrain, but are detected in other regions of the P0 *L3/Lhx8* δHD/δHD mice. Coronal sections of P0 heterozygous (a, b, e and f), WT (i, j and m) and homozygous (c, d, g, h, k, l and n) pups were used for *in situ* hybridization (a–h) or immunohistochemistry (i–n). High-magnification photographs of each boxed area are aligned on the right. *eGFP* mRNA (a–d), *VAChT* mRNA (e–h) and p75 low-affinity NGF receptor (i–l) expression patterns are presented. In the spinal cord of wild-type (m) and δHD/δHD mice (n), ChAT is expressed in the motor neurons (arrows) and in the neurons of the intermediolateral column (arrowhead). The scale bar in (a) represents 1 mm (a and c), 500 μm (b, d, e, g, i, k, m and n), and 200 μm (f, h, j and l).

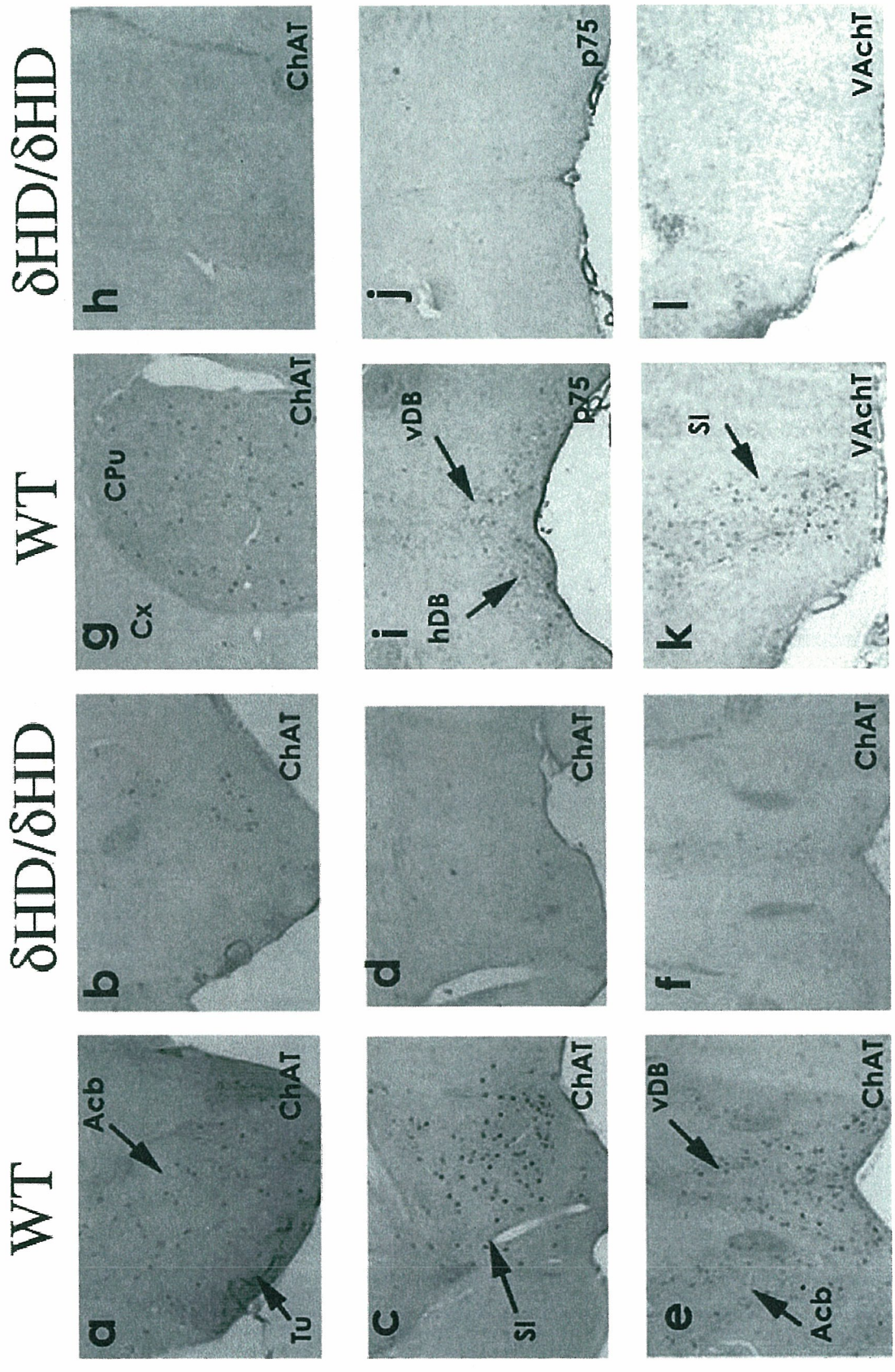

FIG. 5. The number of ChAT-, p75 low-affinity NGF receptor- or vesicular acetylcholine transporter-positive neurons in the basal forebrain are greatly reduced in adult δHD/δHD mice. Coronal sections of WT (a, c, e, g, i and k) and δHD/δHD (b, d, f, h, j, l) mice were used for immunohistochemistry with an anti-ChAT antibody (a–h), anti-p75 low-affinity NGF receptor (i and j) antibody and anti-VAChT antibody (k and l). Acb, accumbens nucleus; Tu, olfactory tubercle; SI, substantia innominata; vDB, vertical limb of the diagonal band; hDB, horizontal limb of the diagonal band; Cpu, caudate putamen; GP, globus pallidus; CX, cerebral cortex. The scale bar in (b) represents 500 μm for all panels.

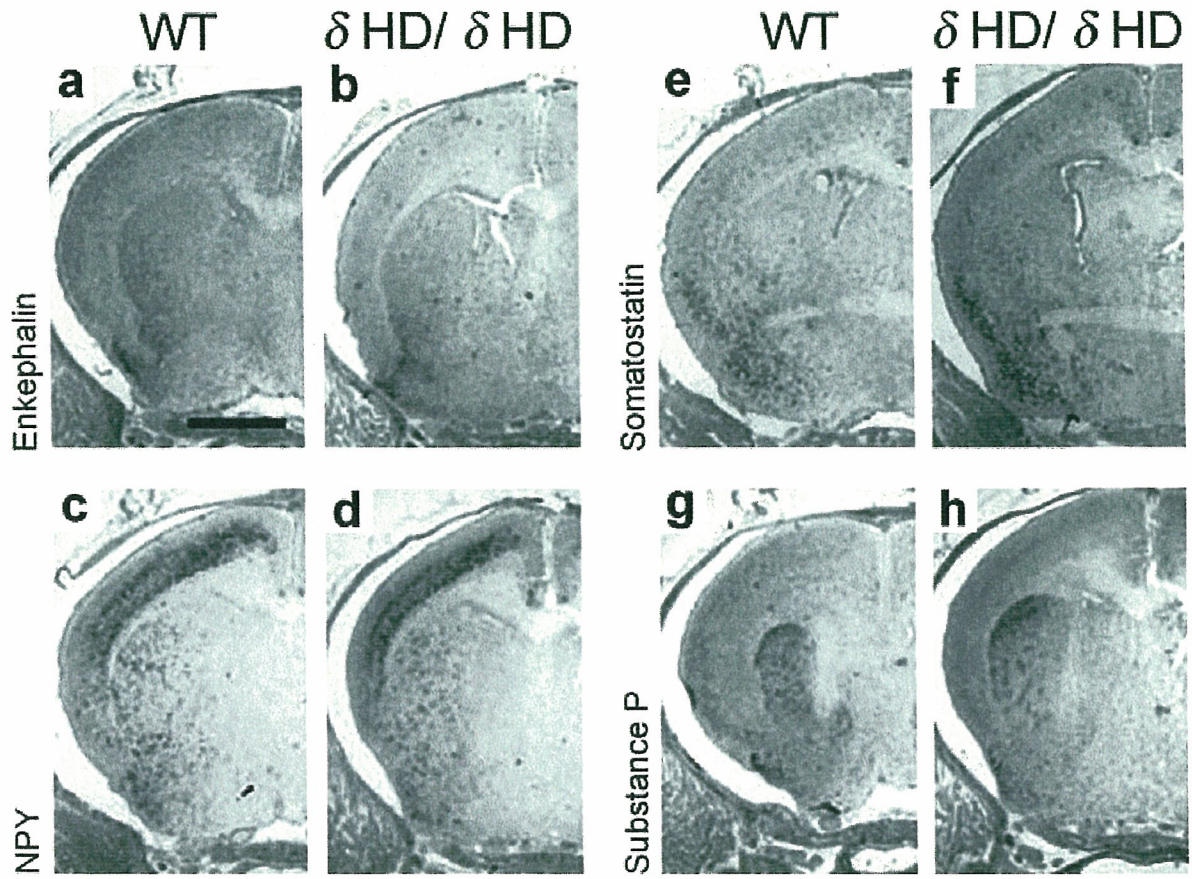

FIG. 6. Almost all neurotransmitter mRNAs distributed in the basal forebrain are expressed normally in the *L3/Lhx8* δHD/δHD mice. Coronal sections of P0 pups from the wild type (WT; a, c, e and g) or P0 homozygous pups (δHD/δHD; b, d, f and h) were hybridized with each probe indicated at the left of each paired panel; *enkephalin* (a, b), *neuropeptide Y* (c and d), *somatostatin* (e and f) and *substance P* (g and h). *NPY*, neuropeptide Y. The scale bar represents 1 mm for all panels.

Interneurons in the olfactory bulb, hippocampus and cerebral cortex were normal in L3/Lhx8 *δHD/δ HD mice*

Most GABAergic interneurons in rodent forebrain are derived from the ventral forebrain; in the olfactory bulb they are derived from the LGE (Anderson *et al.*, 1999); all of them in the hippocampus (Pleasure *et al.*, 2000) and most of them in the neocortex (Anderson *et al.*, 1997) are derived from both the LGE and the MGE.

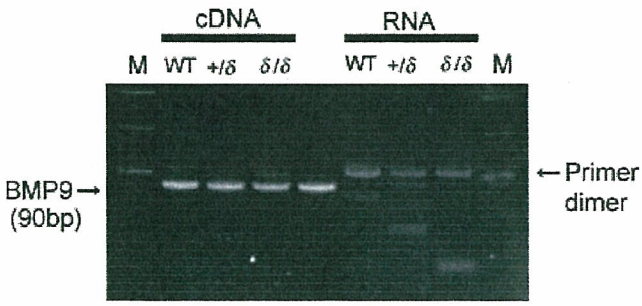

FIG. 7. *BMP9* mRNA is detected by RT-PCR in *L3/Lhx8* δHD/δHD mice. When we use a cDNA template prepared from the basal forebrain of the E14.5 embryos and mouse genomic DNA (G) as a positive control, we can detect a 90-bp PCR product of *BMP9* in all the genotypes (WT, wild type; +/δ, +/δHD; δ/δ, δHD/δHD). As negative controls we use DNase-treated RNAs as a PCR template. In those cases, only the primer dimers or non-specific PCR products are detected. G, genomic DNA; M, molecular marker.

To test the possibility that interneurons derived from ventral telencephalon could be affected by targeted disruption of *L3/Lhx8*, we compared GABAergic neurons in the olfactory bulb (Fig. 8a and b), hippocampus (Fig. 8c and d) and cerebral cortex (Fig. 8e and f) of P0 mice. We detected GABAergic neurons in each brain region of homozygous mice and their numbers and morphologies were similar to those of WT or heterozygous mice. In addition, Lhx6-expressing cells in the cerebral cortex of homozygous mice also migrate from the MGE, in a manner indistinguishable from WT mice (Fig. 8g and h).

Discussion

Different phenotypes between two lines of L3/Lhx8*-targeted mice*

Consistent with a previous study (Zhao *et al.*, 1999), *L3/Lhx8* δHD mice also suffered from cleft palates, but the incidence of cleft palate was much higher (about 95% among δHD/δHD mice) than for *L3/Lhx8−/−* mice (60%). The lower incidence of cleft palate in the *−/−* mice could result from the compensation of the *L3/Lhx8* function by *Lhx6*, because *L3/Lhx8* and *Lhx6* mRNAs were co-expressed in many cells in the MGE and palatal mesenchyme throughout embryonic development (Grigoriou *et al.*, 1998; Zhang *et al.*, 2002). The difference could hardly be attributed to the genetic backgrounds of two lines of *L3/Lhx8*-targeted mice; 129 strain-derived ES cells (R1 used in the previous study of Zhao *et al.*, 1999; D3 used in this study) were

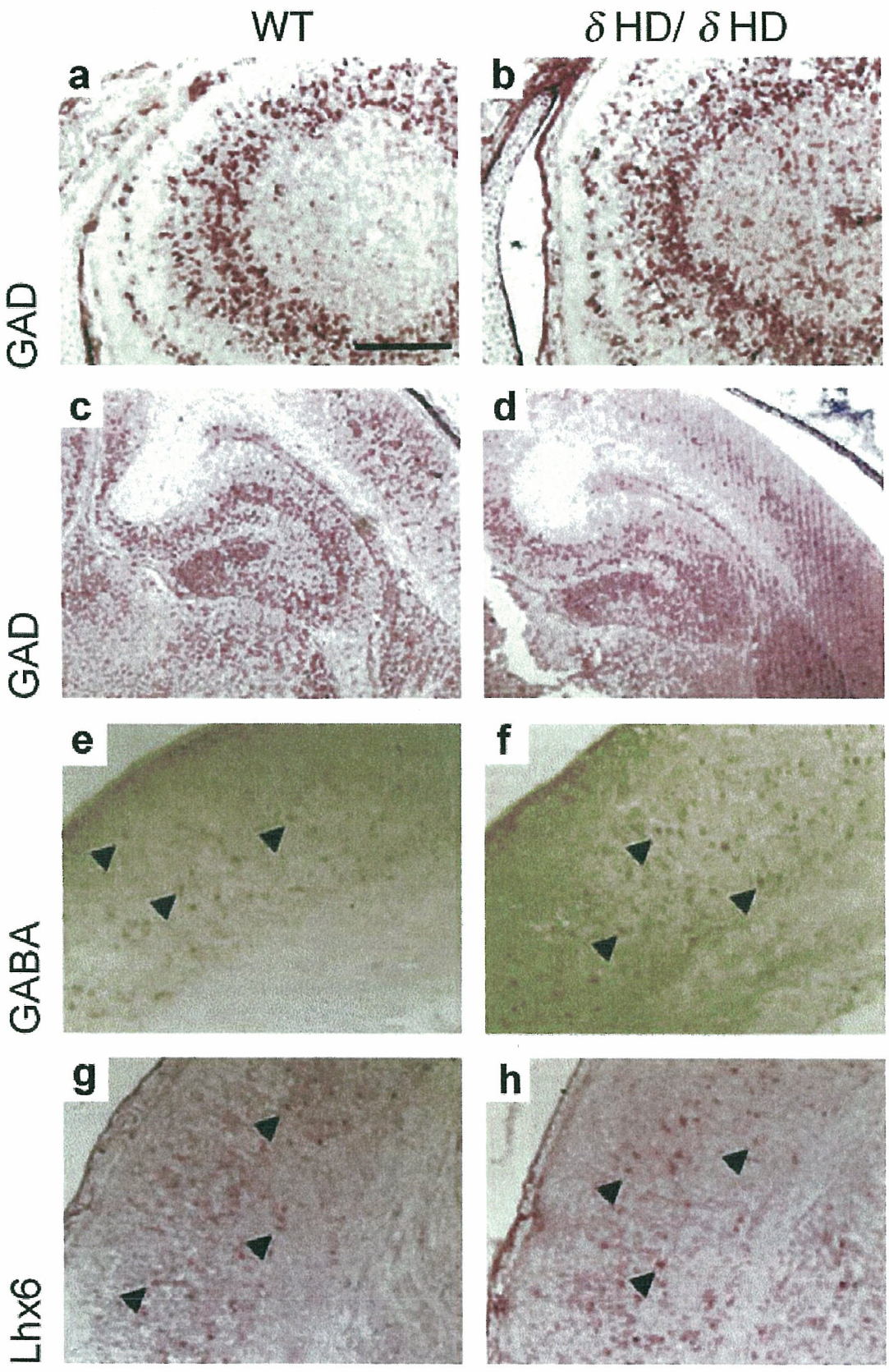
WT
δ HD/ δ HD
a
b
GAD
c
d
GAD
e
f
GABA
g
h
Lhx6

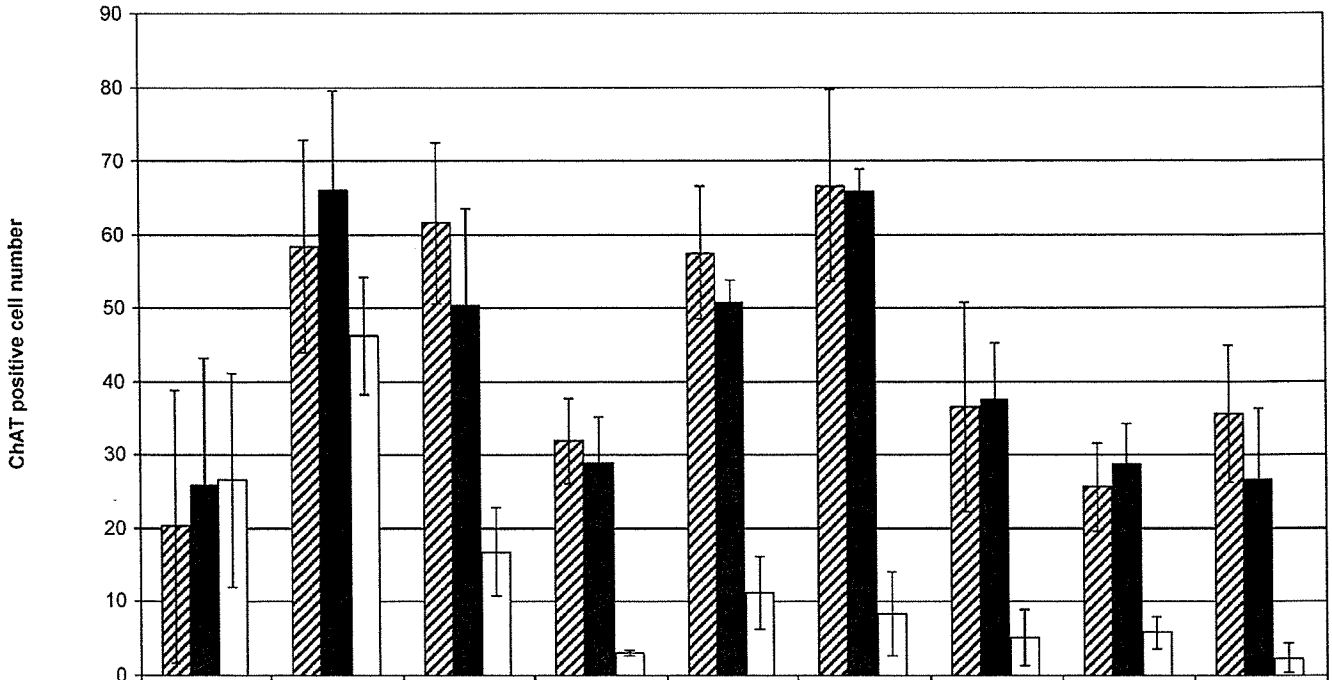

	Tu	Acb	vDB	hDB	MS	Cpu	MCPO	SI	LGP
▨WT	20.27	58.4	61.58	31.93	57.53	66.67	36.6	25.6	35.6
■δHD/+	25.87	66	50.48	29	50.87	65.87	37.47	28.73	26.67
□δHD/δHD	26.6	46.2	16.83	3	11.27	8.4	5.07	5.87	2.33

FIG. 9. ChAT-immunopositive neurons were counted in each nucleus of adult (1 month old) brain and compared between littermates. We counted immunopositive cells in five sections per one animal, and average numbers of three independent brains are indicated as columns (hatched column, WT; filled column, +/δHD; open column, δHD/δHD) and in Table 1. Error bars indicate the standard deviations. Note that the extent of reduction varies between each nucleus in the δHD/δHD mice as compared with the WT mice. Tu, olfactory tubercle; Acb: accumbens nucleus; vDB, vertical limb of the diagonal band nucleus; hDB, horizontal limb of the diagonal band nucleus; MS, medial septum; Cpu, caudate putamen; MCPO, central subnucleus of the medial preoptic nucleus; SI, substantia innominata; LGP, lateral globus pallidus.

employed and back-crossed with C57BL6 in these lines. Although we do not have direct evidence of a dominant-negative effect exerted by the LIM domain-only protein of *L3/Lhx8*, it is likely that we could lessen the compensation of *Lhx6* with our present strategy. Further studies will be required to elucidate the mechanisms underlying the difference.

Specification of cholinergic neurons in the basal forebrain

Several studies suggest that cholinergic neurons in the basal forebrain are heterogeneous. For example, about 13% of the BFCN co-express galanin (Miller *et al.*, 1998) and some cholinergic neurons co-express *Isl-1* whereas others do not (Wang & Liu, 2001). Our study also suggests that L3/Lhx8 plays important roles in the differentiation of some populations of BFCNs, because a great number of the BFCNs were decreased in adult brains of δHD/δHD mice (Fig. 9). While the present study was in preparation, it was reported that *L3/Lhx8−/−* mice showed reduction of BFCNs, albeit to a lesser extent (25–75% reduction) (Zhao *et al.*, 2003) than that of our mice. The lesser reduction of BFCNs in *L3/Lhx8−/−* mice might be attributed to the compensation by Lhx6, as in the palate development. The varied extents of the BFCN reduction between each nucleus of δHD/δHD and *−/−* mice imply a complex nature to the differentiation of cholinergic neurons. For example, the cholinergic neurons in the olfactory tubercle and accumbens nucleus were spared in both lines of targeted mice. These cholinergic neurons could not be descendants of MGE, but of LGE where neither *L3/Lhx8* nor *Lhx6* are expressed; or they do not need both *L3/Lhx8* and *Lhx6* functions. By contrast, cholinergic neurons in the vertical limb of the diagonal band, caudate putamen and globus pallidus require *L3/Lhx8* function for their proper differentiation, because even *L3/Lhx8−/−* mice with possible compensation by *Lhx6* lost up to 75% of their cholinergic neurons (Zhao *et al.*, 2003). The fact that *eGFP* mRNA derived from a recombinant allele of δHD/δHD mice was expressed at P0 in a comparable pattern to that of *L3/Lhx8* mRNA in WT mice (Fig. 4a–d) indicates that BFCN precursors do not undergo apoptosis, but adopt a fate other than that of the cholinergic neuron without *L3/Lhx8* functions. Neurons positive for *enkephalin*, *neuropeptide Y*, *somatostatin*, *substance P*, *GABA* and *galanin* in the basal forebrain appeared unchanged (Fig. 6), although it would be very difficult to detect a 'slight increase' of certain phenotypes at the expense of the BFCNs, numbers of which are small in the

FIG. 8. GABAergic interneurons in the *L3/Lhx8* δHD/δHD mice appear normal. GABAergic interneurons in the olfactory bulb (a and b), hippocampus (c and d) and cerebral cortex (e–h) derived from the basal forebrain are examined. Coronal sections of P0 mice were processed with a *GAD* probe (a–d), *Lhx6* probe (g and h) and anti-GABA antibody (e and f). The scale bar in (a) represents 200 μm (a, b, e, f, g and h) and 500 μm (c and d).

adult brain. Because we failed to detect any significant increase in the number of GAD-positive neurons in the basal forebrain of δHD/δHD mice, we require further study to investoigate this changed fate.

Cholinergic fate is probably determined before birth, because we detected none of the cholinergic markers in the P0 basal forebrain of δHD/δHD mice, whereas we could always observe ChAT-positive BFCNs in P0 WT mice. Consistent with this hypothesis, the expression levels of the two Lhx factors (*L3/Lhx8* and *Lhx6*) are much higher in embryonic than in postnatal brain (Matsumoto *et al.*, 1996; Kimura *et al.*, 1999).

Taking a recent study (Asbreuk *et al.*, 2002) into account, it is likely that sequential and/or simultaneous expressions of the transcription factors, such as *L3/Lhx8*, *Lhx6*, *Isl-1* and *Gbx-1* (and possibly *Gbx-2*, in this study, Fig. 3i and j), are necessary for proper differentiation of BFCNs. The importance of the combination of multiple transcription factors in neuronal differentiation is reinforced by the following data; migrating cortical interneurons expressing *Lhx6*, *GABA* and *neuropeptide Y* (Marin *et al.*, 2001), which derived from the ventral forebrain (MGE and/or LGE), were detected in δHD/δHD mice and their number did not apparently decrease compared with that in WT mice (Fig. 9). These ventral forebrain-derived cortical interneurons might be descendants of precursor cells expressing *Lhx6* (but not *L3/Lhx8*), which distribute in the relatively posterior part of the MGE. BFCNs could be derived mainly from the anterior part of the MGE (*L3/Lhx8* and *Lhx6* double-positive precursors).

The present study provides evidence that *L3/Lhx8* (and possibly *Lhx6*) has important roles in the differentiation of BFCNs. This is the first step toward an understanding of how a neuronal precursor adopts a cholinergic fate.

Acknowledgements

We are grateful to Dr J. L. Rubenstein (UCSF, USA, for the cDNA probe template of *Nkx2.1*, and *Dlx1*, *2* and *5*), Dr T. Taga (Kumamoto University, Japan, for the cDNA probe template of *Lhx6.1*), Dr R. Kuwano (Niigata University, Japan, for the *SA+IRES+PolyA signal* unit), Dr K. Kobayashi (Fukushima Medical University, Japan, for technical assistance) and Dr M. Tohyama (Osaka University Graduate School of Medicine, for his continuous encouragement). This work was supported by a Grant-in-Aid for Young Scientists (B) from the Ministry of Education, Culture, Sports, Science and Technology, Japan.

Abbreviations

BFCNs, sasal forebrain cholinergic neurons; BMPs, bone morphogenetic proteins; ChAT, choline acetyltransferase; (F)ISH, (fluoresence) *in situ* hybridization; GFP, green fluorescent protein; LGE, lateral ganglionic eminence; MGE, medial ganglionic eminence; SVZ, subventricular zone; VAChT, VZ, vesicular acetylcholine transporter; ventricular, zone; WT, wild-type.

References

Anderson, S.A., Eisenstat, D.D., Shi, L. & Rubenstein, J.L. (1997) Interneuron migration from basal forebrain to neocortex: dependence on Dlx genes. *Science*, **278**, 474–476.

Anderson, S., Mione, M., Yun, K. & Rubenstein, J.L. (1999) Differential origins of neocortical projection and local circuit neurons: role of Dlx genes in neocortical interneuronogenesis. *Cereb. Cortex*, **9**, 646–654.

Asbreuk, C.H., van Schaick, H.S., Cox, J.J., Kromkamp, M., Smidt, M.P. & Burbach, J.P. (2002) The homeobox genes Lhx7 and Gbx1 are expressed in the basal forebrain cholinergic system. *Neuroscience*, **109**, 287–298.

Bulfone, A., Puelles, L., Porteus, M.H., Frohman, M.A., Martin, G.R. & Rubenstein, J.L. (1993) Spatially restricted expression of Dlx-1, Dlx-2 (Tes-1), Gbx-2, and Wnt- 3 in the embryonic day 12.5 mouse forebrain defines potential transverse and longitudinal segmental boundaries. *J. Neurosci.*, **13**, 3155–3172.

Casarosa, S., Fode, C. & Guillemot, F. (1999) Mash1 regulates neurogenesis in the ventral telencephalon. *Development*, **126**, 525–534.

Cheng, L., Chen, C.L., Luo, P., Tan, M., Qiu, M., Johnson, R. & Ma, Q. (2003) Lmx1b, Pet-1, and Nkx2.2 coordinately specify serotonergic neurotransmitter phenotype. *J. Neurosci.*, **23**, 9961–9967.

Dawid, I.B., Breen, J.J. & Toyama, R. (1998) LIM domains: multiple roles as adapters and functional modifiers in protein interactions. *Trends Genet.*, **14**, 156–162.

Ding, Y.Q., Marklund, U., Yuan, W., Yin, J., Wegman, L., Ericson, J., Deneris, E., Johnson, R.L. & Chen, Z.F. (2003) Lmx1b is essential for the development of serotonergic neurons. *Nature Neurosci.*, **6**, 933–938.

Eisenstat, D.D., Liu, J.K., Mione, M., Zhong, W., Yu, G., Anderson, S.A., Ghattas, I., Puelles, L. & Rubenstein, J.L. (1999) DLX-1, DLX-2, and DLX-5 expression define distinct stages of basal forebrain differentiation. *J. Comp. Neurol.*, **414**, 217–237.

Ericson, J., Muhr, J., Jessell, T.M. & Edlund, T. (1995) Sonic hedgehog: a common signal for ventral patterning along the rostrocaudal axis of the neural tube. *Int. J. Dev. Biol.*, **39**, 809–816.

Everitt, B.J. & Robbins, T.W. (1997) Central cholinergic systems and cognition. *Annu. Rev. Psychol.*, **48**, 649–684.

Ferrante, R.J., Beal, M.F., Kowall, N.W., Richardson, E.P. Jr & Martin, J.B. (1987) Sparing of acetylcholinesterase-containing striatal neurons in Huntington's disease. *Brain Res.*, **411**, 162–166.

Goridis, C. & Brunet, J.F. (1999) Transcriptional control of neurotransmitter phenotype. *Curr. Opin. Neurobiol.*, **9**, 47–53.

Grigoriou, M., Tucker, A.S., Sharpe, P.T. & Pachnis, V. (1998) Expression and regulation of Lhx6 and Lhx7, a novel subfamily of LIM homeodomain encoding genes, suggests a role in mammalian head development. *Development*, **125**, 2063–2074.

Hallonet, M., Hollemann, T., Pieler, T. & Gruss, P. (1999) Vax1, a novel homeobox-containing gene, directs development of the basal forebrain and visual system. *Genes Dev.*, **13**, 3106–3114.

Harada, Y.N., Shiomi, N., Koike, M., Ikawa, M., Okabe, M., Hirota, S., Kitamura, Y., Kitagawa, M., Matsunaga, T., Nikaido, O. & Shiomi, T. (1999) Postnatal growth failure, short life span, and early onset of cellular senescence and subsequent immortalization in mice lacking the xeroderma pigmentosum group G gene. *Mol. Cell Biol.*, **19**, 2366–2372.

Iseki, K., Hagino, S., Mori, T., Zhang, Y., Yokoya, S., Takaki, H., Tase, C., Murakawa, M. & Wanaka, A. (2002) Increased syndecan expression by pleiotrophin and FGF receptor-expressing astrocytes in injured brain tissue. *Glia*, **39**, 1–9.

Kikuchi, Y., Segawa, H., Tokumoto, M., Tsubokawa, T., Hotta, Y., Uyemura, K. & Okamoto, H. (1997) Ocular and cerebellar defects in zebrafish induced by overexpression of the LIM domains of the islet-3 LIM/homeodomain protein. *Neuron*, **18**, 369–382.

Kimura, S., Hara, Y., Pineau, T., Fernandez-Salguero, P., Fox, C.H., Ward, J.M. & Gonzalez, F.J. (1996) The T/ebp null mouse: thyroid-specific enhancer-binding protein is essential for the organogenesis of the thyroid, lung, ventral forebrain, and pituitary. *Genes Dev.*, **10**, 60–69.

Kimura, N., Ueno, M., Nakashima, K. & Taga, T. (1999) A brain region-specific gene product Lhx6.1 interacts with Ldb1 through tandem LIM-domains. *J. Biochem. (Tokyo)*, **126**, 180–187.

Kohtz, J.D., Baker, D.P., Corte, G. & Fishell, G. (1998) Regionalization within the mammalian telencephalon is mediated by changes in responsiveness to Sonic Hedgehog. *Development*, **125**, 5079–5089.

Lopez-Coviella, I., Berse, B., Krauss, R., Thies, R.S. & Blusztajn, J.K. (2000) Induction and maintenance of the neuronal cholinergic phenotype in the central nervous system by BMP-9. *Science*, **289**, 313–316.

Marin, O., Baker, J., Puelles, L. & Rubenstein, J.L. (2002) Patterning of the basal telencephalon and hypothalamus is essential for guidance of cortical projections. *Development*, **129**, 761–773.

Marin, O., Yaron, A., Bagri, A., Tessier-Lavigne, M. & Rubenstein, J.L. (2001) Sorting of striatal and cortical interneurons regulated by semaphorin–neuropilin interactions. *Science*, **293**, 872–875.

Matsumoto, K., Tanaka, T., Furuyama, T., Kashihara, Y., Mori, T., Ishii, N., Kitanaka, J., Takemura, M., Tohyama, M. & Wanaka, A. (1996) L3, a novel murine LIM-homeodomain transcription factor expressed in the ventral telencephalon and the mesenchyme surrounding the oral cavity. *Neurosci. Lett.*, **204**, 113–116.

Miller, M.A., Kolb, P.E., Planas, B. & Raskind, M.A. (1998) Few cholinergic neurons in the rat basal forebrain coexpress galanin messenger RNA. *J. Comp. Neurol.*, **391**, 248–258.

Misawa, H., Nakata, K., Matsuura, J., Nagao, M., Okuda, T. & Haga, T. (2001) Distribution of the high-affinity choline transporter in the central nervous system of the rat. *Neuroscience*, **105**, 87–98.

Nikaido, T., Yokoya, S., Mori, T., Hagino, S., Iseki, K., Zhang, Y., Takeuchi, M., Takaki, H., Kikuchi, S. & Wanaka, A. (2001) Expression of the novel transcription factor OASIS, which belongs to the CREB/ATF family, in mouse embryo with special reference to bone development. *Histochem. Cell Biol.*, **116**, 141–148.

O'Keefe, D.D., Thor, S. & Thomas, J.B. (1998) Function and specificity of LIM domains in *Drosophila* nervous system and wing development. *Development*, **125**, 3915–3923.

Paxinos, G. & Franklin, K.B.J. (2001) *The mouse brain in stereotaxic coordinates.* Academic Press, San Diego, USA.

Pleasure, S.J., Anderson, S., Hevner, R., Bagri, A., Marin, O., Lowenstein, D.H. & Rubenstein, J.L. (2000) Cell migration from the ganglionic eminences is required for the development of hippocampal GABAergic interneurons. *Neuron*, **28**, 727–740.

Saucedo-Cardenas, O., Quintana-Hau, J.D., Le, W.D., Smidt, M.P., Cox, J.J., De Mayo, F., Burbach, J.P. & Conneely, O.M. (1998) Nurr1 is essential for the induction of the dopaminergic phenotype and the survival of ventral mesencephalic late dopaminergic precursor neurons. *Proc. Natl Acad. Sci. USA*, **95**, 4013–4018.

Segawa, H., Miyashita, T., Hirate, Y., Higashijima, S., Chino, N., Uyemura, K., Kikuchi, Y. & Okamoto, H. (2001) Functional repression of Islet-2 by disruption of complex with Ldb impairs peripheral axonal outgrowth in embryonic zebrafish. *Neuron*, **30**, 423–436.

Sussel, L., Marin, O., Kimura, S. & Rubenstein, J.L. (1999) Loss of Nkx2.1 homeobox gene function results in a ventral to dorsal molecular respecification within the basal telencephalon: evidence for a transformation of the pallidum into the striatum. *Development*, **126**, 3359–3370.

Taira, M., Otani, H., Saint-Jeannet, J.P. & Dawid, I.B. (1994) Role of the LIM class homeodomain protein Xlim-1 in neural and muscle induction by the Spemann organizer in *Xenopus*. *Nature*, **372**, 677–679.

Tojo, M., Mori, T., Kiyosawa, H., Honma, Y., Tanno, Y., Kanazawa, K.Y., Yokoya, S., Kaneko, F. & Wanaka, A. (1999) Expression of sonic hedgehog signal transducers, patched and smoothened, in human basal cell carcinoma. *Pathol. Int.*, **49**, 687–694.

Toresson, H., Potter, S.S. & Campbell, K. (2000) Genetic control of dorsal–ventral identity in the telencephalon: opposing roles for Pax6 and Gsh2. *Development*, **127**, 4361–4371.

Wang, H.F. & Liu, F.C. (2001) Developmental restriction of the LIM homeodomain transcription factor Islet-1 expression to cholinergic neurons in the rat striatum. *Neuroscience*, **103**, 999–1016.

Whitehouse, P.J., Price, D.L., Struble, R.G., Clark, A.W., Coyle, J.T. & Delon, M.R. (1982) Alzheimer's disease and senile dementia: loss of neurons in the basal forebrain. *Science*, **215**, 1237–1239.

Yun, K., Potter, S. & Rubenstein, J.L. (2001) Gsh2 and Pax6 play complementary roles in dorsoventral patterning of the mammalian telencephalon. *Development*, **128**, 193–205.

Zetterstrom, R.H., Solomin, L., Jansson, L., Hoffer, B.J., Olson, L. & Perlmann, T. (1997) Dopamine neuron agenesis in Nurr1-deficient mice. *Science*, **276**, 248–250.

Zhang, Y., Mori, T., Takaki, H., Takeuch, M., Iseki, K., Hagino, S., Murakawa, M., Yokoya, S. & Wanaka, A. (2002) Comparison of the expression patterns of two LIM-homeodomain genes, Lhx6 and L3/Lhx8, in the developing palate. *Orthod. Craniofac. Res.*, **5**, 65–70.

Zhao, Y., Guo, Y.J., Tomac, A.C., Taylor, N.R., Grinberg, A., Lee, E.J., Huang, S. & Westphal, H. (1999) Isolated cleft palate in mice with a targeted mutation of the LIM homeobox gene lhx8. *Proc. Natl. Acad. Sci. USA*, **96**, 15002–15006.

Zhao, Y., Marin, O., Hermesz, E., Powell, A., Flames, N., Palkovits, M., Rubenstein, J.L. & Westphal, H. (2003) The LIM-homeobox gene Lhx8 is required for the development of many cholinergic neurons in the mouse forebrain. *Proc. Natl Acad. Sci. USA*, **100**, 9005–9010.

SYNAPSE 53:53–56 (2004)

Short Communication

Ultrastructural Localization of High-Affinity Choline Transporter in the Rat Neuromuscular Junction: Enrichment on Synaptic Vesicles

KAZUKO NAKATA,[1] TAKASHI OKUDA,[2] AND HIDEMI MISAWA[1]*
[1]*Department of Neurology, Tokyo Metropolitan Institute for Neuroscience, Tokyo 183-8526, Japan*
[2]*Department of Neurochemistry, Faculty of Medicine, University of Tokyo, Tokyo 113-0033, Japan*

KEY WORDS acetylcholine; cholinergic neuron; immunoelectron microscopy; trafficking

ABSTRACT In cholinergic neurons, Na^+- and Cl^--dependent, hemicholinium-3-sensitive, high-affinity choline uptake system is thought to be the rate-limiting step in acetylcholine (ACh) synthesis. The system is highly regulated by neuronal activity; the choline uptake is increased by a condition in which ACh release is favored. Here we analyzed the ultrastructural localization of the high-affinity choline transporter (CHT) in the rat neuromuscular junctions with two separate antibodies. The majority (>90%) of immunogold labeling of CHT was observed on synaptic vesicles rather than the presynaptic plasma membrane. Less than 5% of the gold-silver particles were associated with the plasma membrane, and more than 70% of such particles were localized within or in close vicinity to presynaptic active zones. Our morphological data support the recent hypothesis that trafficking of CHT from synaptic vesicles to the plasma membrane couples neuronal activity and choline uptake. **Synapse 53:53–56, 2004.**

Acetylcholine (ACh) is a major neurotransmitter both in the central and peripheral nervous system. ACh is synthesized from choline and acetyl-CoA by the enzyme choline acetyltransferase (ChAT), which is specifically expressed in cholinergic neurons. For efficient and sustained neurotransmission, cholinergic neurons are endowed with a unique high-affinity choline uptake (HACU) system (Haga, 1971; Haga and Noda, 1973; Kuhar et al., 1973; Kuhar and Murrin, 1978; Tucek, 1985; Yamamura and Snyder, 1972). The HACU activity is Na^+- and Cl^--dependent and inhibited by hemicholinium-3 (HC-3) (Kuhar and Zarbin, 1978; Yamamura and Snyder, 1972, 1973). Studies using brain synaptosomes and slices demonstrated that the HACU system is the rate-limiting step in ACh synthesis, and the HACU activity is highly regulated by neuronal activity (Murrin et al., 1977; Saltarelli et al., 1987; Simon and Kuhar, 1975). Owing to a lack of structural information, the cellular mechanism governing the activity-dependent regulation of the HACU activity remains largely unknown.

By using information from the *Caenorhabditis elegans* Genome Project and expression screening in *Xenopus laevis* oocytes, Okuda et al. (2000) first cloned the nematode high-affinity choline transporter (cho-1). Later, mammalian cDNA clones encoding the high-affinity choline transporter (CHT) were isolated and characterized from rat (Okuda et al., 2000), human (Apparsundaram et al., 2000; Okuda and Haga, 2000), and mouse (Apparsundaram et al., 2001). Light microscopic immunohistochemical studies in rodents (Ferguson et al., 2003; Lips et al., 2002; Misawa et al., 2001) and primates (Kobayashi et al., 2002; Kus et al., 2003; Misawa et al., 2001) showed that CHT was uniquely expressed in all major cholinergic cell groups and enriched in their projection fields, being consistent with the known function of CHT at cholinergic axon terminals. Recently, Ferguson et al. (2003) showed, by using

*Correspondence to: Hidemi Misawa, Department of Neurology, Tokyo Metropolitan Institute for Neuroscience, 2-6 Musashidai, Fuchu City, Tokyo 183-8526, Japan. E-mail: hmisawa@tmin.ac.jp

Received 26 January 2004; Accepted 8 March 2004

DOI 10.1002/syn.20029

Published online 6 May 2004 in Wiley InterScience (www.interscience.wiley.com).

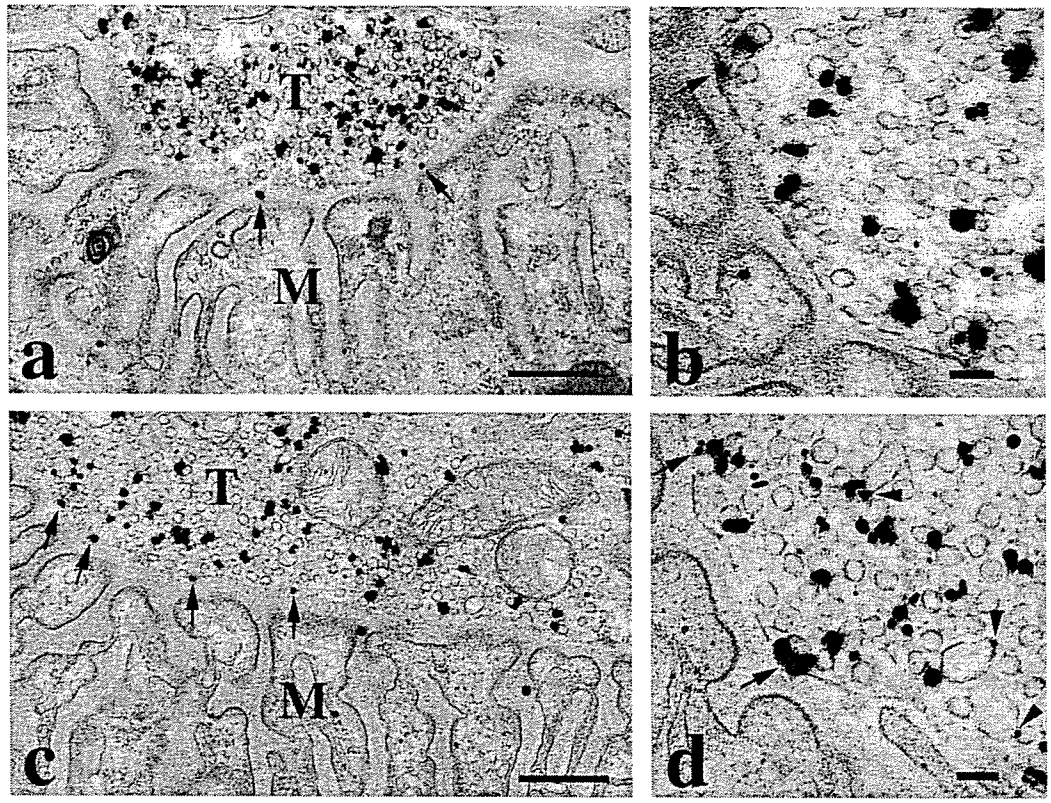

Fig. 1. Immunoelectron photomicrographs of neuromuscular junctions in the rat diaphragms labeled with anti-CHT antibody against GST-fusion protein (**a, b**) or with anti-CHT antibody against C-terminal peptide (**c, d**). The silver-enhanced gold particles are mostly associated with synaptic vesicles, and occasionally with the plasma membrane (arrows) in the phrenic motor axon terminals (T) forming typical neuromuscular junctions with the diaphragm muscle (M). Some endosome-like irregular vesicles (arrowheads in d) are associated with the immuno-particles. Scale bars = 500 nm in a, c (low-magnification images); 100 nm in b, d (high-magnification images, different section from a and c).

immunoelectron microscopy and biochemical characterization, that CHT was enriched on small presynaptic vesicles in the cholinergic terminals in the rat facial motor nucleus and striatum. In the present study, we analyzed the ultrastructural localization of CHT in rat neuromuscular junctions (NMJ) with two separate antibodies against CHT.

All the procedures conducted in this study were approved by the Institutional Animal Care and Use Committee at Tokyo Metropolitan Institute for Neuroscience. Six adult female Sprague Dawley rats (250–300 g; SLC, Shizuoka, Japan) were used. Animals were deeply anesthetized with sodium pentobarbital (150 mg/kg) and perfused through the aortic cone at a flow rate of 20 ml/min with 50 ml of 0.1 M phosphate buffer pH 7.4 containing 0.9% NaCl (PBS), followed by 250 ml of 4% paraformaldehyde in 0.1 M phosphate buffer (PB, pH 7.4) containing 0.1% glutaraldehyde and 0.2% saturated picric acid. Whole diaphragms were removed and postfixed in the same fixative for 2 h at 4°C. After fixation, the diaphragms were cut into 1.5–2-mm-square pieces and blocked in 3% normal goat serum (NGS; Vector Labs, Burlingame, CA) in 0.02 M PBS containing 0.01% saponin (PBS-S) overnight at 4°C. The diaphragm pieces were then incubated for 3 days at 4°C with 80 ng/ml of affinity-purified anti-CHT rabbit IgG against the rat CHT C-terminal region (amino acids 502–580) fused to glutathione S-transferase (GST) (Misawa et al., 2001) or with 25 ng/ml of affinity-purified anti-CHT rabbit IgG against the CHT peptide (C-terminal 15 amino acids; Kobayashi et al., 2002) in 3% NGS in PBS-S. After several washes in PBS-S, the pieces were incubated in a 1:100 dilution of affinity-purified goat anti-rabbit Fab′ fragments conjugated to 1.4-nm colloidal gold particles (NANOGOLD-Fab′ conjugates; Nanoprobes, Yaphank, NY) in 3% NGS in PBS-S for 16 h at 4°C. The pieces were rinsed in PBS, postfixed for 15 min in 1% glutaraldehyde in PBS, and rinsed in distilled water. The conjugated gold particles were silver-enhanced in the dark with HQ Silver Enhancement Kit (Nanoprobes) for 2 min at room temperature. The labeled sections were fixed in 1% osmium tetroxide for 30 min at 4°C, dehydrated through a graded series of ethanol solutions and finally propylene oxide, and embedded in Quetol 812 (Nissin EM, Tokyo, Japan). Once the resin had polymerized, approximately 3-μm sections were cut and examined with a light microscope and the regions containing NMJ were selected for electron microscopy. The sections were re-embedded in Quetol 812, and then cut into ultrathin

sections on an ultramicrotome (MT6000; RMC Inc., Tucson, AZ). The ultrathin sections were counterstained with Reynold's lead citrate and uranyl acetate and examined with an electron microscope (H7500; Hitachi, Tokyo, Japan) at 20,000× magnification. To quantify immunogold labeling in subcellular compartments in the motor nerve terminal, electron microscopic images were printed out and silver-gold particles were counted. A total of 12 presynaptic terminals with good morphological preservation were analyzed.

The two polyclonal antibodies specific to CHT used in this study exhibited almost the same pattern of CHT localization in the motor nerve terminals (Fig. 1). Surprisingly, the majority of CHT immunogold-silver particles were located on synaptic vesicles; only a small portion of CHT immunoreactivity was associated with the plasma membrane. The synaptic vesicles in motor axon terminals labeled with the silver grains had usually spherical and occasionally endosome-like irregular morphology (Fig. 1d). We counted a total of 1,139 silver-enhanced gold particles and categorized them as either synaptic vesicle-associated, plasma membrane-associated, or others (associated with mitochondria, cytoplasm, or unidentified compartments) (Fig. 2a). The plasma membrane-associated particles were counted when the immuno-particles were located within 50 nm from the plasma membrane. Among the plasma membrane-associated CHT immuno-particles (48 particles), a large portion (>70%) was located within or in close vicinity (within 100 nm) to the active zones, where the nerve terminal directly opposes junctional folds in the postsynaptic membrane (Figs. 1, 2b). We categorized 41% of the linear distance of the presynaptic membrane (16.4 μm) as "active zones" out of the total length of the presynaptic membrane analyzed (40 μm).

We report here the first description of the immunoelectron microscopic localization of CHT in the rat NMJ, the best characterized of all cholinergic synapses (Hall and Sanes, 1993; Sanes and Lichtman, 1999). Two kinds of polyclonal antibody against CHT gave the same pattern of labeling in NMJ; >90% on the synaptic vesicles and <5% on the plasma membranes. Furthermore, the stereotypic well-characterized structure of the NMJ enabled us to quantify a fine localization of CHT in the presynaptic plasma membrane; CHT immuno-particles were preferentially found at the presynaptic active zones or its vicinity. The active zones are sites where synaptic vesicles fuse to the plasma membrane and release their content (ACh) to the synaptic cleft. The preferential localization of CHT at the active zones possibly suggests that CHT is delivered to the plasma membrane from synaptic vesicles via membrane fusion. Recently, Ferguson et al. (2003) reported, by using immunoelectron microscopy, that a large portion of CHT immunoreactivity was localized on synaptic vesicles in cholinergic presynaptic terminals in the

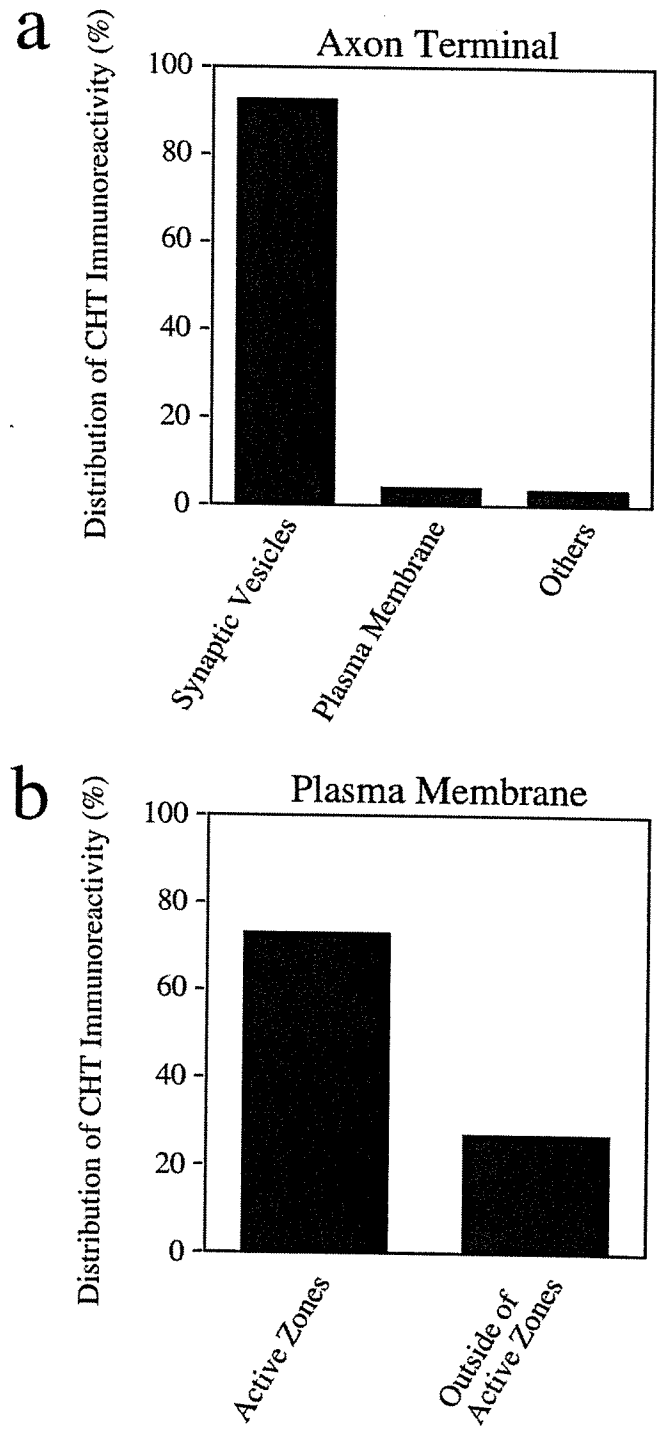

Fig. 2. Quantitative analysis of the subcellular distribution of CHT immunoreactivity in the phrenic motor axon terminals (**a**) and within the plasma membrane (**b**). Percentage of immunogold particles is calculated by dividing the number associated with each compartment by the total number of particles counted (a, 1,139; b, 48). We counted 736 particles in 7 terminals stained with anti-CHT antibody against GST-fusion protein (30 particles were on the plasma membrane), and 403 particles in 5 terminals stained with anti-CHT antibody against C-terminal peptide (18 particles on the plasma membrane).

facial motor nucleus and striatum. Moreover, by using biochemical characterization, they presented a novel and intriguing hypothesis that neuronal activity triggers CHT trafficking from synaptic vesicles to the plasma membrane where levels of choline-uptake couples to ACh release. Although we cannot rule out the possibility that CHT functions as a vesicular transporter for choline or as yet unidentified substrates on synaptic vesicles, the immunoelectron microscopic data presented here strongly support Ferguson et al.'s (2003) hypothesis.

Our immunoelectron microscopic analysis demonstrates that only a small portion (<5%) of CHT immunoreactivity is associated with the plasma membrane. This low percentage possibly suggests that CHT undergoes efficient recovery from the plasma membrane to intracellular vesicles by an endocytic pathway. Furthermore, we occasionally observed CHT immuno-particles on pleiomorphic vesicles, possible endocytic organelles (Fig. 1d). In accordance with this observation, recent CHT transfection analyses in cultured cells demonstrate that CHT is efficiently and constitutively internalized by a clathrin-mediated endocytic pathway (Ferguson and Blakely, 2004; Ribeiro et al., 2003).

In aging and in Alzheimer's disease, dysfuction of cholinergic neurons is well correlated with a decline in cognitive function, and acetylcholinesterase (AChE) inhibitors are so far the only class of drugs for treatment of these disorders. The activity-dependent trafficking model will provide a basis for CHT as a potential new therapeutic target for these disorders.

ACKNOWLEDGMENTS

We thank Dr. Masumi Ichikawa and Mrs. Kyoko Ajiki (Tokyo Metropolitan Institute for Neuroscience) for their valuable advice on immunoelectron microscopy, and Dr. Christian Dillon (University College London) and Dr. Ryosuke Takahashi (RIKEN Brain Science Institute, Saitama, Japan) for their critical reading of the manuscript.

REFERENCES

Apparsundaram S, Ferguson SM, George Jr AL, Blakely RD. 2000. Molecular cloning of a human, hemicholinium-3-sensitive choline transporter. Biochem Biophys Res Commun 276:862–867.

Apparsundaram S, Ferguson SM, Blakely RD. 2001. Molecular cloning and characterization of a murine hemicholinium-3-sensitive choline transporter. Biochem Soc Trans 29:711–716.

Ferguson SM, Blakely RD. 2004. The choline transporter resurfaces: new roles for synaptic vesicles? Mol Interv 4:22–37.

Ferguson SM, Savchenko V, Apparsundaram S, Zwick M, Wright J, Heilman CJ, Yi H, Levey AI, Blakely RD. 2003. Vesicular localization and activity-dependent trafficking of presynaptic choline transporters. J Neurosci 23:9697–9709.

Haga T. 1971. Synthesis and release of [^{14}C]acetylcholine in synaptosomes. J Neurochem 18:781–798.

Haga T, Noda H. 1973. Choline uptake system of rat brain synaptosomes. Biochim Biophys Acta 291:564–575.

Hall ZW, Sanes JR. 1993. Synaptic structure and development: the neuromuscular junction. Cell 72:99–121.

Kobayashi Y, Okuda T, Fujioka Y, Matsumura G, Nishimura Y, Haga T. 2002. Distribution of the high-affinity choline transporter in the human and macaque monkey spinal cord. Neurosci Lett 317:25–28.

Kuhar MJ, Murrin LC. 1978. Sodium-dependent, high-affinity choline uptake. J Neurochem 30:15–21.

Kuhar MJ, Zarbin MA. 1978. Synaptosomal transport: a chloride dependence for choline, GABA, glycine and several other compounds. J Neurochem 31:251–256.

Kuhar MJ, Sethy VH, Roth RH, Aghajanian GK. 1973. Choline: selective accumulation by central cholinergic neurons. J Neurochem 20:581–593.

Kus L, Borys E, Chu YP, Ferguson SM, Blakely RD, Emborg ME, Kordower JH, Levey AI, Mufson EJ. 2003. Distribution of high affinity choline transporter immunoreactivity in the primate central nervous system. J Comp Neurol 463:341–357.

Lips KS, Pfeil U, Haberberger RV, Kummer W. 2002. Localization of the high-affinity choline transporter-1 in the rat skeletal motor unit. Cell Tissue Res 307:275–280.

Misawa H, Nakata K, Matsuura J, Nagao M, Okuda T, Haga T. 2001. Distribution of the high-affinity choline transporter in the central nervous system of the rat. Neuroscience 105:87–98.

Murrin LC, DeHaven RN, Kuhar MJ. 1977. On the relationship between [^{3}H]choline uptake activation and [^{3}H]acetylcholine release. J Neurochem 29:681–687.

Okuda T, Haga T. 2000. Functional characterization of the human high-affinity choline transporter. FEBS Lett 484:92–97.

Okuda T, Haga T, Kanai Y, Endou H, Ishihara T, Katsura I. 2000. Identification and characterization of the high-affinity choline transporter. Nature Neurosci 3:120–125.

Ribeiro FM, Alves-Silva J, Volknandt W, Martins-Silva C, Mahmud H, Wilhelm A, Gomez MV, Rylett RJ, Ferguson SS, Prado VF, Prado MA. 2003. The hemicholinium-3 sensitive high affinity choline transporter is internalized by clathrin-mediated endocytosis and is present in endosomes and synaptic vesicles. J Neurochem 87:136–146.

Saltarelli MD, Lowenstein PR, Coyle JT. 1987. Rapid in vivo modulation of [^{3}H]hemicholinium-3 binding sites in rat striatal slices. Eur J Pharmacol 135:35–40.

Sanes JR, Lichtman JW. 1999. Development of the vertebrate neuromuscular junction. Annu Rev Neurosci 22:389–442.

Simon JR, Kuhar MG. 1975. Impulse-flow regulation of high affinity choline uptake in brain cholinergic nerve terminals. Nature 255: 162–163.

Tucek S. 1985. Regulation of acetylcholine synthesis in the brain. J Neurochem 44:11–24.

Yamamura HI, Snyder SH. 1972. Choline: high-affinity uptake by rat brain synaptosomes. Science 178:626–628.

Yamamura HI, Snyder SH. 1973. High affinity transport of choline into synaptosomes of rat brain. J Neurochem 21:1355–1374.

Neuropathology 2005; **25**, 381–387

Workshop: Recent Advances in Motor Neuron Disease

Is motoneuronal cell death in amyotrophic lateral sclerosis apoptosis?

Mineo Yamazaki,[1,2] Eisaku Esumi[3] and Imaharu Nakano[4]

[1]Division of Neurology, 2nd Department of Internal Medicine, Nippon Medical School, [2]Department of Neuropathology, Tokyo Metropolitan Institute for Neuroscience, [3]Department of Neurology, Tokyo Tama Hospital, Tokyo and [4]Department of Neurology, Jichi Medical School, Tochigi, Japan

To clarify the controversy concerning whether the cell death of motor neurons in ALS is apoptosis, we investigated the expression of Apaf-1 and caspase-9 mRNA in spinal cord tissue obained at autopsy from patients with ALS and controls using RT-PCR; the presence of *in situ* nuclear DNA fragmentation in motor neurons by the TdT-mediated dUTP-biotin nick end-labeling (TUNEL) method; and immunocytochemical localization of Apaf-1 and caspase-3, which are known as promotors of apoptotic processes. Although Apaf-1 and caspase-9 mRNAs levels were increased in ALS, Apaf-1 immunoreactivity (IR) showed no significant difference between ALS and the control, and caspase-3 IR was not observed in ALS motoneurons, casting doubt on the notion that motor neurons in ALS undergo death by the classic apoptotic pathway. Although TUNEL-positive motor neurons were frequently observed in the anterior horn in ALS, these neurons always showed an atrophic cell body with a shrunken and pyknotic nucleus, indicating that they were at the terminal stage of degeneration. No apoptotic bodies were seen. These findings suggest that the mechanism of motor neuronal cell death in ALS might not be apoptosis, but some other as yet unidentified mechanism.

Key words: amyotrophic lateral sclerosis, Apaf-1, apoptosis, caspase, cell death, DNA fragmentation.

INTRODUCTION

Since the discovery of missense mutations in the chromosome 21 gene which encodes copper/zinc superoxide dismutase-1 (SOD1) in the dominantly inherited ALS family,[1–4] ALS research has focused on this SOD1 gene mutation.[5–9] A number of authors have proposed the possibility of programmed cell death, termed apoptosis, in the motor neurons in SOD1 transgenic mice, and suggested that the same cell death processes also occur in classic ALS in humans.

The definition of apoptosis is so fuzzy, however, as to confound attempts to interpret the results of apoptosis studies over a range of degenerative diseases. This lack of clarity is reflected in inconsistencies in the biochemical and morphological features of motoneuronal cell death observed in SOD1 transgenic mice and in patients with ALS.[10–16]

Several recent investigations of motor neuronal cell death in ALS have focused on caspases and related proteins in SOD1 transgenic mice.[17–20] Caspases are generated in the form of pro-enzymes (inactive form), and are activated by proteolysis to form active complexes which kill neurons via the apoptosis process. The caspases examined in the present study are thought to be associated with mitochondria and to be active in the final common pathway of the caspase cascade. Cytochrome C (Apaf-2) and Apaf-1 are discharged together from mitochondria, and form a complex with caspase-9 through caspase recruitment domain in the presence of dATP. As a result, caspase-9 is changed to the activated form, which in turn activates caspase-3, which finally induces cell death.

To clarify whether apoptosis is in fact associated with the cell death of motoneurons in ALS patients, we studied the presence of DNA fragmentation, the definitive sign of apoptosis, in these cells. In addition, we also analyzed Apaf-1 and caspase-9 mRNA, and immunocytochemically investigated Apaf-1 and caspase-3 in spinal motoneurons in ALS patients.

Correspondence: Mineo Yamazaki, MD, PhD, The 2nd Department of Internal Medicine, Nippon Medical School, 1-1-5 Sendagi, Bunkyo-ku, Tokyo 113-8602, Japan. Email: yamazaki@nms.ac.jp

Received 26 May 2005; accepted 30 May 2005.

MATERIALS AND METHODS

Tissue preparation

The brain and cervical and lumbar segments of the spinal cord were rapidly obtained at autopsy of patients with ALS ($n = 3$), disease controls ($n = 2$, ossification of the posterior longitudinal ligament and MSA) and non-neurological disease controls ($n = 2$, acute myocardial infarction and adrenal gland cancer). All ALS patients showed symptoms of upper and lower motor neuron involvement and fulfilled the pathological criteria of ALS. The tissues obtained at autopsy were preserved, frozen at –80°C until analysis. For the TdT-mediated dUTP-biotin nick end-labeling (TUNEL) method, sections were made from formalin-fixed and paraffin-embedded blocks of the appropriate regions.

RT-PCR method

Total mRNA was isolated from the cerebral cortex (area 17), putamen and spinal cord of ALS patients. Poly A+ mRNA was controlled using a Quickprep mRNA purification kit (Amersham Pharmacia Biotech, Uppsala, Sweden). RT-PCR was performed using the following primers specific to *Apaf-1* and *caspase-9* genes. The sense and antisense primers for *Apaf-1* were 5′-ACATCACGAA TCTTTCCCGC-3′, corresponding to APPN, and 5′-AACACTTCACTATCACTTCC-3′, corresponding to APPC. The primers used for *caspase-9* were 5′-GCCATG GACGAAGCGGATCGGCGG-3′ (sense) and 5′-GGC CTGGATGAAAAAGAGCTGGG-3′ (antisense). PCR was performed with a synthetic first-strand cDNA template. Amplification was continued for 35 cycles (1 min denaturation at 94°C, 1 min annealing at 55°C, 2 min extension at 72°C).

Immunohistochemistry

Immunohistochemical staining was performed using mouse monoclonal anti-Apaf-1 antibody (MAB868; R & D systems, Minneapolis, MN, USA), rabbit polyclonal anti-CPP32 antibody[21] and mouse monoclonal anticaspase-3 antibody (sc-7272; Santa Cruz Biotechnology, CA, USA). Frozen sections were incubated with 3% hydrogen peroxide for 30 min to block endogenous peroxidase activity. The sections were incubated with the antibodies at 4°C overnight and immunoreactivity was visualized with a Histostain SP kit (Zymed, San Francisco, CA, USA).

TUNEL method

Formalin-fixed, paraffin-embedded lumbar cord specimens from six ALS patients were examined in comparison with those from four controls. To facilitate the earliest possible detection of changes in motor neurons, these six cases were selected from among more than 50 ALS cases for their relatively well-preserved anterior horn cells. Mean age of the ALS and control (three with cerebral infarction and one with Marchiafava-Bignami disease) patients was 67 years (range 50–84 years) and 50 years (range 18–70 years), respectively.

DNA fragmentation was detected by the TUNEL method, using an *in situ* cell death detection kit (Boehringer-Mannheim, Indianapolis, MN, USA). Negative controls were examined using TUNEL reaction solution without TdT or fluorescein dUTP. Feasibility of the nuclear labeling of cells by the TUNEL method was confirmed in intestinal tissue obtained at autopsy of patients with malignant lymphoma. After oligonucleosomal DNA cleavages were labeled, photos of each TUNEL-positive neuron were taken, the same specimens were stained with HE, and TUNEL-positive neurons identified from the

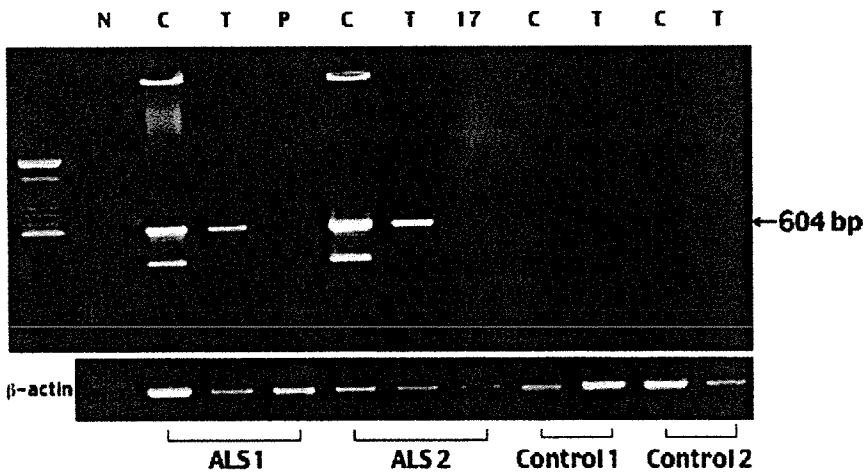

Fig. 1 Detection of Apaf-1 mRNA in the brains of control and ALS patients. β-actin mRNA in the same samples was used as control. The Apaf-1 mRNA band was detected in the cervical and thoracic cord, and was compared with cerebral cortex and putamen in patients with ALS (N: negative control, C: C8, T: Th12, P: putamen, 17: area 17).

photos were cytopathologically observed. TUNEL-positive spinal motor neurons and all anterior motor neurons in all sections were counted, and the frequency of TUNEL-positive spinal motor neurons was measured.

RESULTS

PT-PCR

PCR using primers to amplify *Apaf-1* clearly revealed positive bands of Apaf-1 mRNA in the cervical (C8) and thoracic cord (T12) in patients with ALS, but not in the cerebral cortex and putamen as such. In contrast, Apaf-1 mRNA was scarcely detected in the spinal cord of control cases (Fig. 1). Apaf-1 mRNA was clearly expressed in the putamen and cervical cord of patients with MSA (Fig. 2). The caspase-9 mRNA band was detected in the spinal cord of ALS patients and putamen and cervical cord of MSA patients, but was hardly seen in control cases (Fig. 3).

Immunocytochemistry

To determine whether Apaf-1 and caspase-3 are activated in ALS, control and ALS brains were immunostained with anti-Apaf-1 and anticaspase-3 antibodies. For Apaf-1, anterior horn motoneurons in control and ALS spinal cords showed weak cytoplasmic staining for Apaf-1, whereas ALS brains showed no significant differences to control brains (Fig. 4a,b). Immunolabeling using antibodies specific to caspase-3, rabbit polyclonal anti-CPP32 antibody (Fig. 4c,d) and mouse monoclonal anticaspase-3 antibody (Fig. 4e,f) revealed only scarce caspase-3 immunoreactivity in motor neurons in control and ALS brains.

TUNEL method

TUNEL-positive motor neurons in the anterior horn were observed in three of six ALS cases, whereas in control cases only two TUNEL-positive neurons were seen, one each in two cases. The TUNEL-positive motor neurons were atrophic and round in both groups, without large cell processes. They were filled with lipofuscin and the nucleus was eccentric, flat and pyknotic (Fig. 5a,b). Although TUNEL-positive motor neurons with Lewy body-like hyaline inclusions were occasionally found (Fig. 5c,d), no TUNEL-positive neurons carrying Bunina bodies were observed.

Not all atrophic anterior horn neurons were TUNEL-positive; some had TUNEL-negative nuclei, which were always a generally round shape with a light nucleoplasm. (Fig. 5e,f). However, most TUNEL-negative neurons were of normal size and had many processes in their cell bodies. TUNEL-positive motor neurons represented 5.3–8.9% of

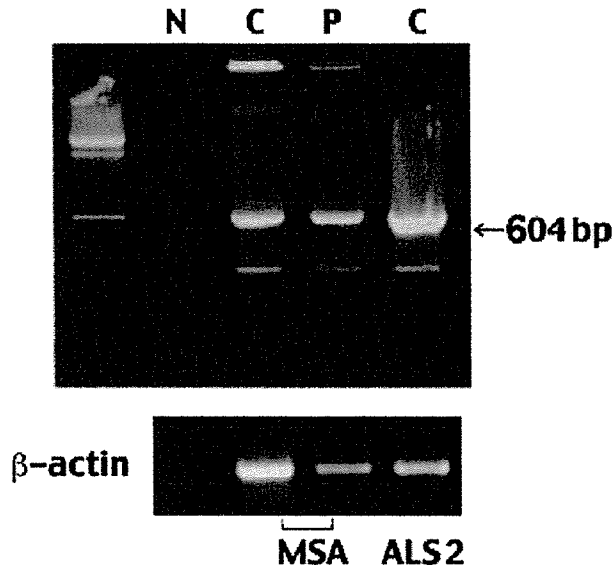

Fig. 2 Detection of Apaf-1 mRNA in the brains of MSA patients. Apaf-1 mRNA was expressed in the putamen and cervical cord of a patient with MSA (N: negative control, C: C8, P: putamen).

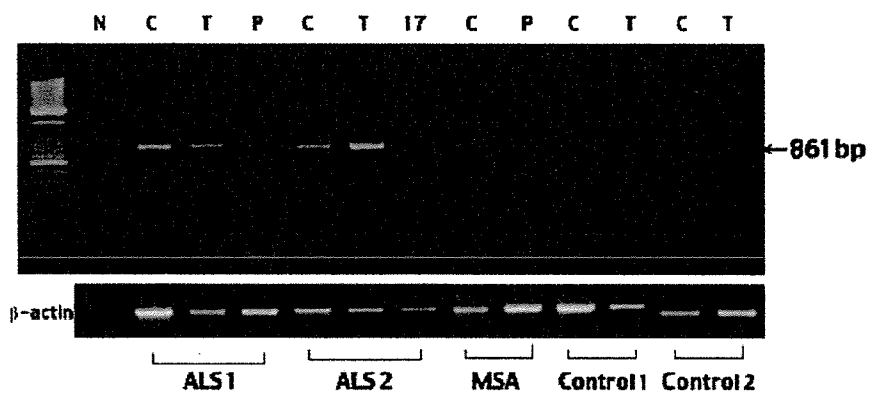

Fig. 3 Expression of caspase-9 mRNA in control, MSA and ALS brains. The caspase-9 mRNA band was detected in the spinal cord of ALS patients and in the putamen and cervical cord of MSA patients, but not in control case tissues (N: negative control, C: C8, T: Th12, P: putamen, 17: area 17).

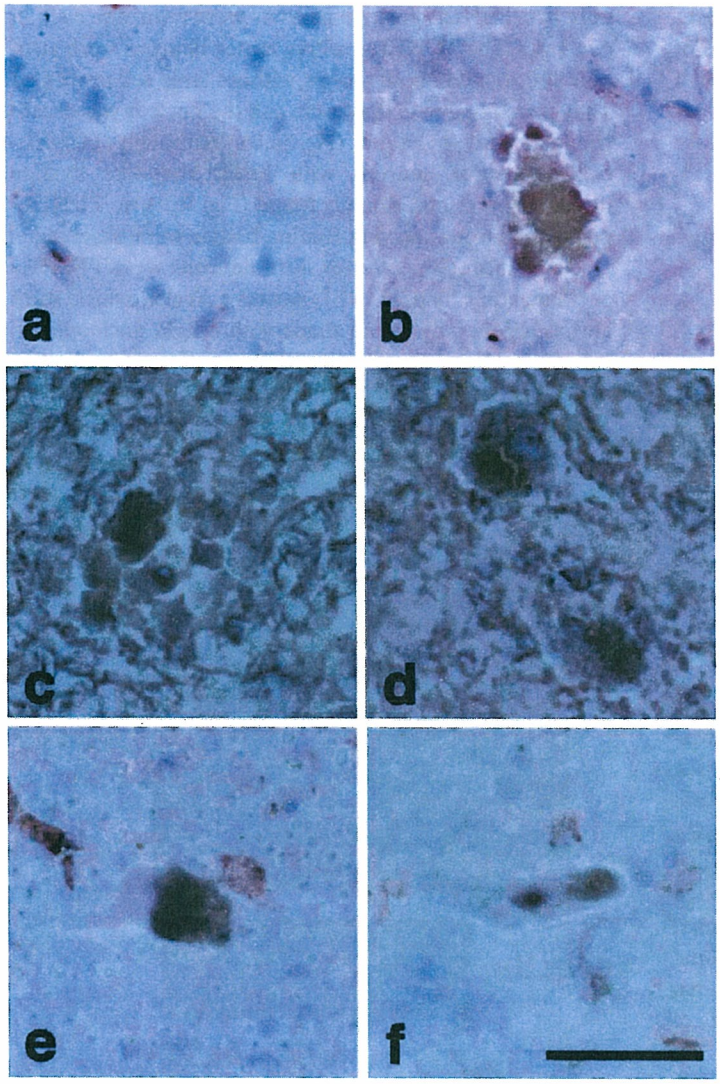

Fig. 4 Immunohistochemical expression of Apaf-1 and caspase-3 in the spinal cord of control and ALS patients. (a,b) No difference in Apaf-1 immunostaining between ALS (a) and control (b) cervical cords (C8). (c,d) Immunolabeling using rabbit polyclonal anti-CPP32 antibody showed no immunoreactivity in anterior horn neurons of control (c) or ALS (d) lumbar cords (L5). (e,f) Mouse monoclonal anticaspase-3 antibody revealed almost no immunoreactivity of caspase-3 in motor neurons in ossification of the posterior longitudinal ligament (e) or ALS (f) cervical cords (C8). Bar, 100 μm.

all anterior horn neurons (Table 1), and all motor neurons with a normal appearance were TUNEL-negative. No apoptotic bodies were seen in any ALS patient specimen.

DISCUSSION

For several reasons, the findings of this study on whether neurons in ALS undergo apoptosis were inconclusive. Although mRNAs of Apaf-1 and caspase-9 were apparently expressed in ALS brains, indicating that apoptosis through *Apaf-1* and *caspase-9* may be, at least to some extent, involved in this neuronal cell death, expression was not restricted to the ALS brain but was also recognized to some degree in the MSA brain. Further, we could not determine whether Apaf-1 mRNA and caspase-9 mRNA in the ALS brains were expressed by neurons, glia, or both. Indeed, our immunocytochemical investigation of Apaf-1, caspase-9 and caspase-3 failed to show any substantial increase in the production of these proteins in ALS over control brains. Against these findings, however, it was recently reported that caspase-9 is activated in spinal motor neurons of ALS patients.[22] It thus remains unclear whether caspase-9 is activated in motor neurons of ALS brains. In our study, caspase-9 mRNA was expressed in ALS brains and was clearly activated in motor neurons of the ALS spinal cord. However, our data also suggest that caspase-3 was not activated in the spinal motor neuron, and it was unlikely that the apoptotic cascade from caspase-9 to caspase-3 was present.

The phenomenon apoptosis was originally defined as fulfilling the following conditions: (i) DNA fragmentation;

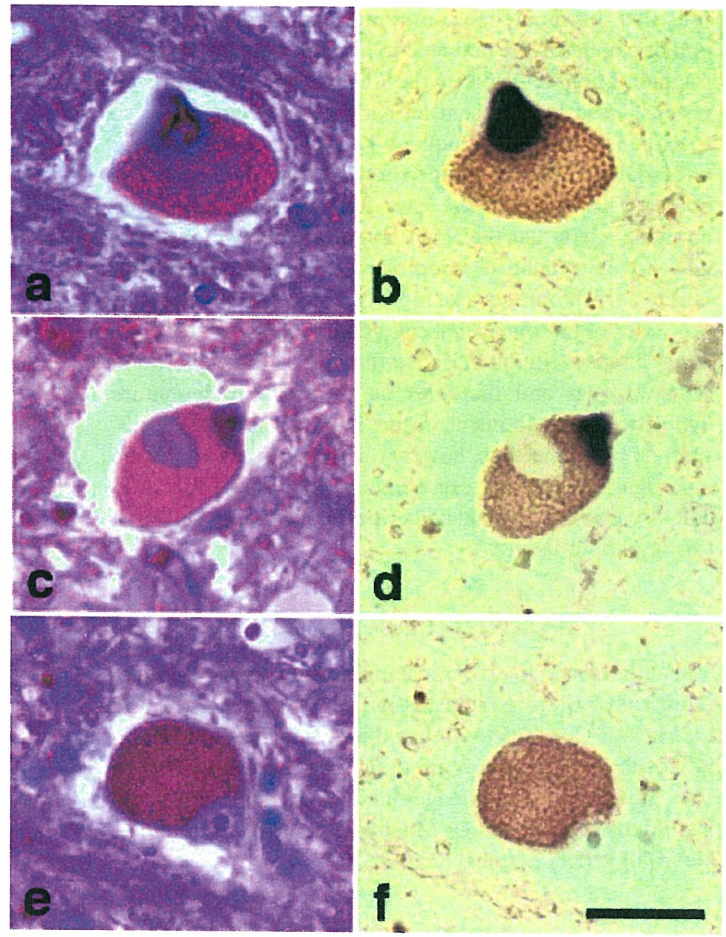

Fig. 5 TdT-mediateddUTP-biotinnickend-labeling (TUNEL) staining of anterior horn neurons in ALS patients. (a,b) A TUNEL-positive lumbar motor neuron is seen (case 1). The cell body is round and filled with lipofuscin. The same section stained with HE stain (a) and the TUNEL method (b). (c,d) TUNEL staining was occasionally observed in motor neurons with hyaline inclusions. (e,f) Some TUNEL-negative anterior horn neurons were atrophic and filled with lipofuscin. Bar, 50 μm.

Table 1 Positive TdT-mediated dUTP-biotin nick end-labeling (TUNEL) of ALS spinal motor neurons

Case	Age (years), sex	Total no. neurons (no.sections)	TUNEL-positive neurons	Mean % positive per section
1	61, female	486 (10)	26	5.3
2	81, female	219 (5)	13	5.9
3	67, male	202 (10)	18	8.9

and (ii) nuclear fragmentation and cellular budding (the presence of apoptotic bodies). Given the inconclusive PCR and immunocytology results here, we also checked whether the morphological changes of motor neurons in ALS were compatible with this definition. Results using the TUNEL method showed the presence of *in situ* DNA fragmentation in 5–9% of spinal motor neurons in ALS patients. If this DNA fragmentation does in fact represent a process of apoptosis, and if apoptotic cell death in motoneurons proceeds over a few hours as seen in other organs, this high proportion of TUNEL-positive cells would result in the total mathematical disappearance of spinal motor neurons in only a few months, with patients of course dying long before. In reality, however, the typical clinical course of several years before death means that one or both of the above assumptions is wrong. Although the possibility that apoptosis occurs more slowly in *in situ* motor neurons than other organ cells cannot be denied, *in vitro* studies using neuronal cell cultures[23] and our present finding that all TUNEL-positive neurons had shrunken pyknotic nuclei suggest that the mechanism of motor neuronal cell death in ALS represents a different process to apoptosis as defined above.

Moreover, it has been reported that the formation of apoptotic bodies was completed within several minutes in cells of a culture system.[24] Further, *in vivo*, apoptotic bodies disappear within only a few hours after formation in organs such as the liver.[25] If this is the case for motoneu-